nature cancer

Article

https://doi.org/10.1038/s43018-023-00669-x

Bacteria and bacteriophage consortia are associated with protective intestinal metabolites in patients receiving stem cell transplantation

Received: 8 March 2023

Accepted: 13 October 2023

Published online: 03 January 2024

Check for updates

A list of authors and their affiliations appears at the end of the paper

The microbiome is a predictor of clinical outcome in patients receiving allogeneic hematopoietic stem cell transplantation (allo-SCT). Microbiota-derived metabolites can modulate these outcomes. How bacteria, fungi and viruses contribute to the production of intestinal metabolites is still unclear. We combined amplicon sequencing, viral metagenomics and targeted metabolomics from stool samples of patients receiving allo-SCT ($n = 78$) and uncovered a microbiome signature of *Lachnospiraceae* and *Oscillospiraceae* and their associated bacteriophages, correlating with the production of immunomodulatory metabolites (IMMs). Moreover, we established the IMM risk index (IMM-RI), which was associated with improved survival and reduced relapse. A high abundance of short-chain fatty acid-biosynthesis pathways, specifically butyric acid via butyryl-coenzyme A (CoA):acetate CoA-transferase (*BCoAT*, which catalyzes EC 2.8.3.8) was detected in IMM-RI low-risk patients, and virome genome assembly identified two bacteriophages encoding *BCoAT* as an auxiliary metabolic gene. In conclusion, our study identifies a microbiome signature associated with protective IMMs and provides a rationale for considering metabolite-producing consortia and metabolite formulations as microbiome-based therapies.

Allo-SCT offers a cure for many hematological diseases. Its success is limited by severe morbidity and mortality associated with acute graft-versus-host disease (GvHD)[1]. In patients receiving allo-SCT, the intestinal bacterial microbiome is altered by loss of diversity and domination of disease-related taxa[2–4]. Multiple factors contribute to this GvHD-related microbial signature, such as antibiotics, (radio) chemotherapy and malnutrition[5,6]. Alterations of bacterial communities influence the pathophysiology of GvHD and affect the outcome of patients receiving allo-SCT[6–10].

Microbiota-derived metabolites such as short-chain fatty acids (SCFAs) and tryptophan derivatives such as indoles and secondary bile acids (BAs) have been shown to exert immunomodulatory effects (for example, via modulation of regulatory T cell (T_{reg}) function or induction of type I interferon (IFN-I) signaling) and tissue homeostatic functions (for example, by acting on intestinal epithelial cells (IECs))[11–13]. Propionic and butyric acid, indole-3-carboxaldehyde (ICA) and deoxycholic acid (DCA) have been associated with protection against GvHD in mice and humans[12]. Additionally, alterations of bacteria together with metabolites, such as loss of specific anaerobic commensals and a decrease in intestinal SCFA levels, have been linked to GvHD severity in patients receiving allo-SCT[14].

Microbiota-derived metabolites have been analyzed in the blood of patients with acute[15] and chronic GvHD[16]. However, in humans, the majority of SCFAs are metabolized on first pass[17], and, while only 2% of

e-mail: e.orberg@tum.de; hendrik.poeck@ukr.de

https://doi.org/10.1038/s43018-023-00669-x

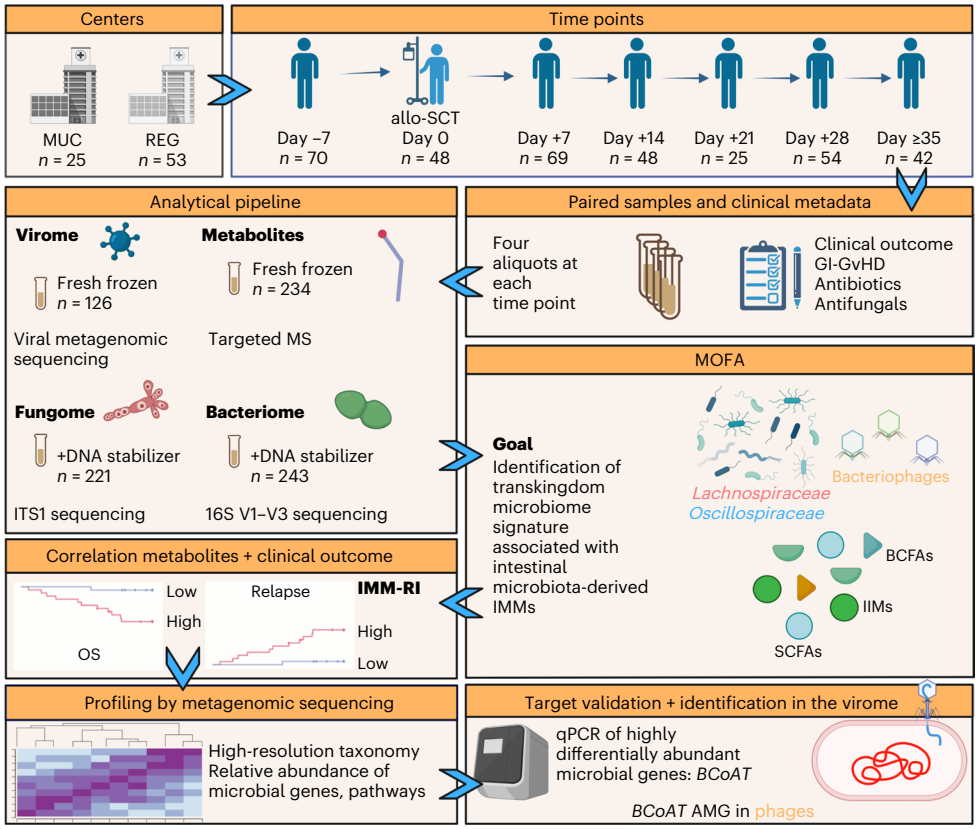

Fig. 1 | Study design and sampling scheme. Graphical representation of allo-SCT centers including patient numbers per center, sampling time points including number of patients per time point, sampling scheme including processing and storage, sample numbers per multiomic modality and downstream analytics. MS, mass spectrometry. Created with https://www.biorender.com.

intestinal butyric acid becomes systemically available[18], it is essential locally for maintaining intestinal homeostasis, where it fuels colonocytes, promotes mucus secretion and enhances expression of tight junction proteins[19].

The intestinal microbiome is composed not only of bacteria but also fungi, viruses, protozoa and archaea. Prokaryotic viruses, that is, bacteriophages, encoding auxiliary metabolite genes (AMGs) can modulate bacterial metabolism while imparting fitness benefits to themselves[20,21]. Bacteriophage-infected bacteria undergo phage-directed metabolism and exhibit distinct physiology compared to their uninfected peers[22]. Although analyses of the human gut virome remain challenging due to the high degree of viral sequence diversity and continual discovery of new viruses by metagenomics[23], a recent study linked picobirnaviruses to severe gastrointestinal (GI)-GvHD[24]. How dynamic shifts in these kingdoms, for example, after antibiotic exposure (ABX)[6] or at the onset of GvHD, affect local, intestinal metabolite profiles and contribute to clinical outcome needs to be further investigated[24].

Results

Allo-SCT alters bacterial, viral and metabolite profiles

In this prospective, observational, longitudinal cohort, we profiled bacterial, fungal and viral communities together with microbiota-derived metabolites in 78 patients receiving allo-SCT at two German academic hospitals (Munich (MUC) and Regensburg (REG)). Starting at day −7 relative to the day of transplantation (day 0), weekly stool sampling was performed, resulting in a mean of four samples per patient (Fig. 1). Acute leukemia, followed by myelodysplastic syndrome, were the most common indications for transplantation (Supplementary Table 1). The majority of patients received reduced-intensity conditioning regimens before transplantation (88% and 87% at MUC and REG, respectively) and were engrafted with unmodified peripheral blood stem cells (96% and 75%) from unrelated donors (72% and 74%).

Longitudinal profiling of the intestinal microbiome and metabolome demonstrated a loss of diversity in bacterial and viral communities, which was lowest at day +14 (Fig. 2a). Across both centers, fungal diversity did not decline during the peri-engraftment period. In line with this, bacterial load, quantified by real-time PCR, decreased after allo-SCT, while fungal load remained stable (Extended Data Fig. 1a). Viral load was not quantifiable due to the absence of viral housekeeping genes.

β-diversity analysis revealed that bacterial communities at day −7 were significantly different from those at late time points (days +7–28; Extended Data Fig. 1b). Likewise, the virome of patients sampled at day −7 clustered separately from that at day +28. For the fungome, no differential clustering pattern according to time point was observed. Identical antifungal therapeutic (but different prophylactic) standards between MUC and REG (Supplementary Table 2) did not impact β-diversity (Extended Data Fig. 1c).

Next, we screened for known IMM classes (SCFAs, branched-chain fatty acids (BCFAs), IFN-I-inducing metabolites (IIMs) including tryptophan derivatives and the flavonoid metabolism byproduct desaminotyrosine (DAT) as well as BAs) in stool samples. By targeted mass spectrometry (MS), we analyzed a total of 57 intestinal metabolites: panel 1 consisted of SCFAs, BCFAs, IIMs and lactic acid. Panel 2 consisted of primary bile acids (PBAs) and secondary BAs (SBAs).

At early time points (days −7 to 0), patients had abundant expression of panel 1 metabolites (Fig. 2b and Extended Data Fig. 2a), which declined at late time points. Lactic acid, which was enriched at late time points, was the exception. In panel 2, the PBAs cholic acid (CA) and chenodeoxycholic acid (CDCA) were enriched at day +28, and so were the CA-derived SBAs ursodeoxycholic acid (UDCA) and

https://doi.org/10.1038/s43018-023-00669-x

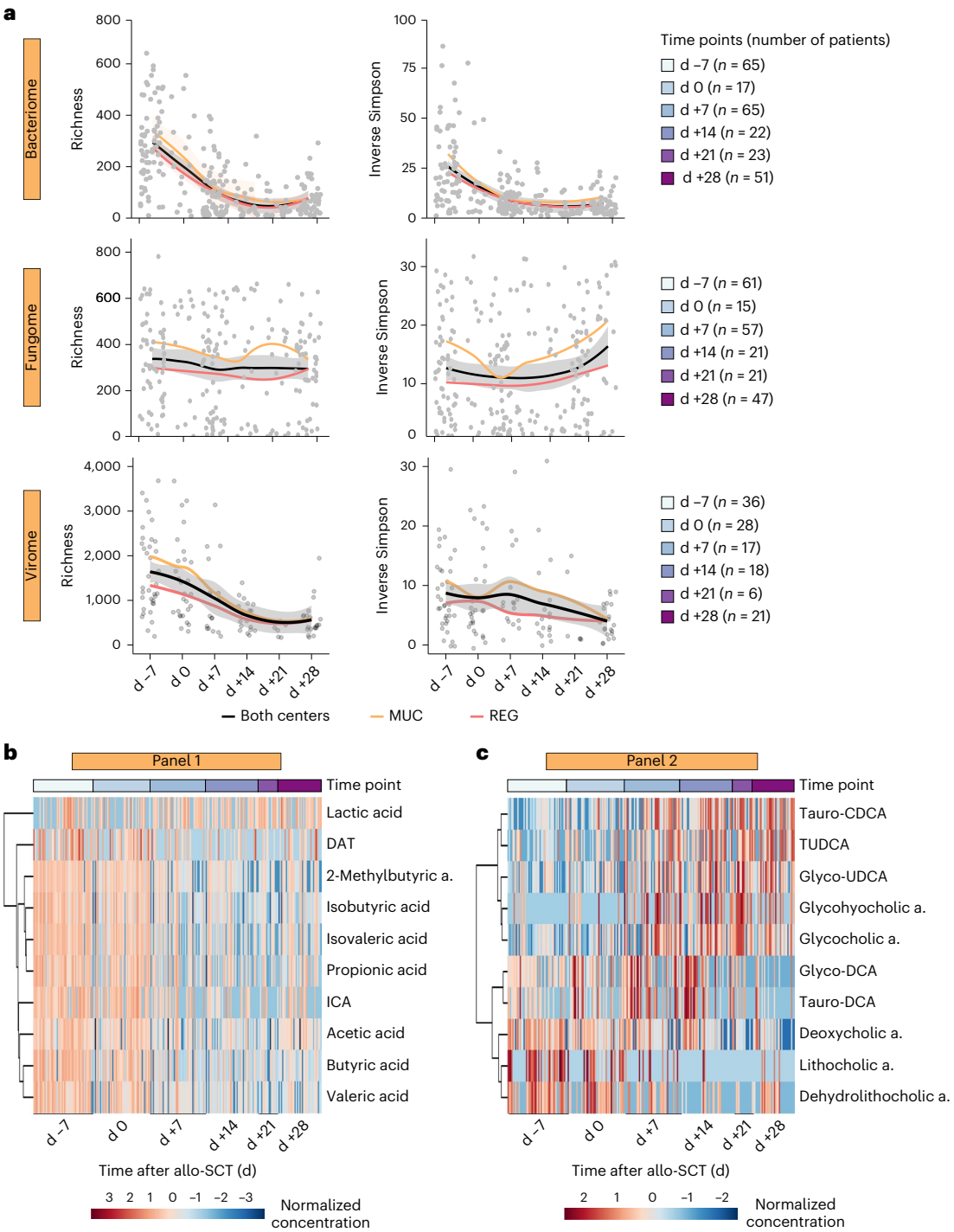

Fig. 2 | Longitudinal dynamics of the intestinal bacteriome, fungome, virome and metabolome in patients receiving allo-SCT. a, Intestinal microbiome composition in the bacteriome (16S V1-V3 amplicon sequencing, $n = 266$ samples), the fungome (ITS1 amplicon sequencing, $n = 245$ samples) and the virome (viral metagenomic shotgun sequencing, $n = 138$ samples) at time points relative to allo-SCT (day 0) by α-diversity indices (richness by the number of observed zero-radius operational taxonomic units (zOTUs) and inverse Simpson's diversity index, respectively). Solid lines represent the smoothed conditional means for the entire cohort (black), those at MUC (orange) or those at REG (red), calculated by locally weighted regression using the locally estimated scatterplot smoothing method. Gray shading indicates the 95% confidence interval of the respective α-diversity index for the entire cohort. Each individual patient stool sample is plotted as a gray dot superimposed on the graph. The number of patients at each time point is indicated to the right. d, day. **b**,**c**, Heatmaps of intestinal concentration of microbiota-derived metabolites measured by MS (in µmol per g dry feces) normalized by log transformation (base 10) in stool samples ($n = 269$ samples) of patients receiving allo-SCT ordered by time points relative to allo-SCT (day 0). **b**, Displayed are SCFAs, BCFAs and IIMs, that is, DAT and ICA as well as lactic acid. a., acid. **c**, Shown are SBAs. In each panel, the top ten metabolites are shown, selected based on highest significance in ANOVA group comparisons between time points. Clustering is based on metabolite expression patterns using the Ward algorithm. The distance measure is Euclidean.

tauroursodeoxycholic acid (TUDCA) (Fig. 2c and Extended Data Fig. 2b). By contrast, SBAs with known immunomodulatory functions, such as CA-derived DCA as well as CDCA-derived lithocholic acid (LCA)[13], were enriched only at early time points.

Principal-component analysis showed that metabolite expression profiles at day −7 were significantly different from those at late time points (Extended Data Fig. 2c,d). We observed overlapping clusters between days +7 and 28, suggesting that the peri-engraftment state was metabolite unique and persisted until at least 1 month after allo-SCT.

Bacteria and bacteriophages are associated with IMMs

We employed multiomic factor analysis (MOFA; explained in Supplementary Note 1) to integrate four omic modalities: datasets obtained from (1) bacterial 16S and (2) fungal internal transcribed spacer (ITS)1 amplicon sequencing, (3) viral metagenomic sequencing of isolated virus-like particles (VLPs) and (4) intestinal metabolite levels identified and quantified by MS.

By MOFA, we identified complex covariation patterns within and across the bacteriome, the virome and the metabolome (Fig. 3a). In these omic modalities, approximately 40% of total variance was explained by ten factors (Fig. 3b). By contrast, MOFA explained less than 10% of variance in the fungome. Factors 1, 3 and 4 explained a large fraction of variance within the bacteriome, the variance explained within the virome was divided between factors 1 through 5, and factors 1–3 explained the most variance within the metabolome. For factor 1, variance observed within the bacteriome and the metabolome was explained broadly by a wide range of features exerting moderate effects (Fig. 3c). Because factors 1 and 3 explained a large proportion of the total variance across the cohort, captured covariations within bacterial and viral kingdoms as well as metabolites and were positively correlated with intestinal concentrations of IMMs (Extended Data Fig. 3a), they were the focus for downstream analysis.

Factor 1 was linked to the genera *Ruminococcus*, *Subdoligranulum* and others within the *Oscillospiraceae* family of obligate anaerobes (weight > 1; Fig. 3d). Only *Enterococcus* was negatively correlated with factor 1. All viral features identified in factor 1 were bacteriophages and were negatively correlated. Some of these viral clusters, for example, VC334, were predicted to infect *Enterococcus*, and we observed a strong correlation with *Enterococcus* (Extended Data Fig. 4a). Panel 1 metabolites had the highest feature weights and were positively correlated, including the SCFAs butyric, propionic and valeric acid and the BCFAs 2-methylbutyric, isovaleric and isobutyric acid as well as the tryptophan metabolite ICA. Panel 2 metabolites had both positive (with the immunomodulatory SBAs DCA and the LCA derivative dehydro-LCA) and negative (with the SBAs UDCA and TUDCA) correlations.

Factor 3 was linked to the genera *Lachnoclostridium*, *Anaerostipes*, *Blautia* and others from *Lachnospiraceae*, a family of obligate anaerobes that ferment plant polysaccharides (weight > 0.5; Fig. 3e). As in factor 1, all top viral features were bacteriophages. In contrast to factor 1, the viral clusters BAC3, VC62, VC64 and VC27 were positively correlated and were associated with genera in the *Lachnospiraceae* family (Extended Data Fig. 4b). Factor 3 was positively correlated with many panel 2 metabolites, including the SBA ursocholic acid, the oxidized SBAs 3- and 7-dehydrocholic acid as well as the PBAs CA and CDCA. From panel 1, we detected a positive correlation with DAT, SCFAs and BCFAs.

Even though factor 4 only explained a small fraction of variance in the metabolome, we noted the covariation of *Bacteroides* and *Parabacteroides* with the viral clusters VC191 and VC612 together with propionic acid levels (Extended Data Figs. 3b and 4c).

MEFISTO[25] is a toolbox for factor analysis of multimodal data with spatial or temporal dependencies. Given that we analyzed a longitudinal cohort, temporal dependencies existed between samples. Therefore, we employed MEFISTO to assess the extent to which the variation captured by the factors could be attributed to time. The highest scale value assigned by MEFISTO was 0.19 for factor 1, followed by 0.05 for factor 7, suggesting only a low time dependency of the factors (Extended Data Fig. 3c).

For both factors, the top 15 viral features identified by MOFA were bacteriophages, which target bacterial hosts. Indeed, when we queried the intestinal virome across our cohort, we confirmed that bacteriophages were in much higher abundance than eukaryotic viruses, including human DNA viruses (Supplementary Fig. 1), both before and after allo-SCT (Extended Data Fig. 3d). In addition, our viral metagenomic sequencing pipeline identified numerous unclassified viral contigs.

In light of recent reports suggesting that bacteriophages can modulate metabolic processes in bacteria[21], we correlated the top bacterial and viral features and linked their abundance to the normalized concentration of intestinal IMMs. We observed significant correlations with a Pearson's correlation coefficient ranging from $R = 0.5$ to $R = 0.7$ for genera within the *Oscillospiraceae* and *Lachnospiraceae* families including *Ruminococcus* and *Blautia* with the bacteriophages BAC3, VC62 and VC27. Intestinal metabolite concentrations, shown as an example for butyric acid (Fig. 3f), were high when bacteria and bacteriophages were co-abundant. Likewise, we observed high intestinal concentrations of propionic acid and the BCFA isovaleric acid as well as the IIMs DAT and ICA when both bacteria and bacteriophages were present in high abundance (Extended Data Fig. 5a–d).

In sum, MOFA-identified factors 1 and 3 described a functional microbiome signature linking intestinal SCFAs, BCFAs and IIMs with bacterial taxa from the *Oscillospiraceae* and *Lachnospiraceae* families and bacteriophages.

The IMM-RI predicts outcome

The intestinal microbiome is a predictor of outcome in patients receiving allo-SCT[7]. Thus, we asked whether the microbiome signature

Fig. 3 | MOFA identifies bacterial and bacteriophage consortia associated with intestinal IMMs. a, Bar plot of the total variance explained by MOFA (in percent) within each omic modality. Exact percentage values are superimposed on the bars. **b**, Heatmap of variance (var.) explained by individual MOFA-identified factors, which capture major sources of variability within and across omics datasets. Rows show the percentage of variance explained by a given factor. Columns indicate the omic modality. **c**, Bar plot showing the fraction of significant associations between the features of each omic modality and factors 1, 3 and 4. Correlations between features and factors were analyzed with Pearson's correlation coefficient. *P* values were corrected for multiple testing by the false discovery-rate (FDR) approach. Statistical significance was called at $P \leq 0.05$. Exact fraction values are superimposed on the bars. **d**, List of high-weight factor features within each omic modality in descending order according to their corresponding feature weight. For each factor, MOFA learns a 'weight' as a measure of importance of every feature contained within that factor, hence enabling interpretation of the variation captured by that factor[43]. A larger weight indicates a higher correlation with that factor, while the positive or negative sign indicates the directionality of that variation; that is, '+' indicates a positive association, and '−' indicates a negative association. Shown are the top 15 features in the bacteriome, the virome and the metabolome for factor 1. Viral taxa are listed by viral cluster name. Blue or red font coloring indicates membership within the *Oscillospiraceae* and *Lachnospiraceae* families. **e**, As in **d** for factor 3. Orange coloring indicates bacteriophages that were correlated with *Oscillospiraceae* and *Lachnospiraceae*. DHCA, dehydrocholic acid. **f**, Scatterplots of top features within factor 3, plotting the normalized abundance of bacteriophages at the species level (*y* axis) against that of bacterial taxa at the genus level (*x* axis). Dots represent samples from individual patients at different time points (91 samples from 45 patients). Dots are colored by intestinal levels of butyric acid or in gray if no butyric acid data were available. Normalized concentrations of metabolites are indicated in the adjacent color legend. Associations between bacterial genera and viral species were analyzed by Pearson correlation and linear regression. The correlation coefficient *R* as well as the associated *P* value are provided in each plot. The regression line is drawn in gray, and the 95% confidence interval of the regression line is shaded in gray.

https://doi.org/10.1038/s43018-023-00669-x

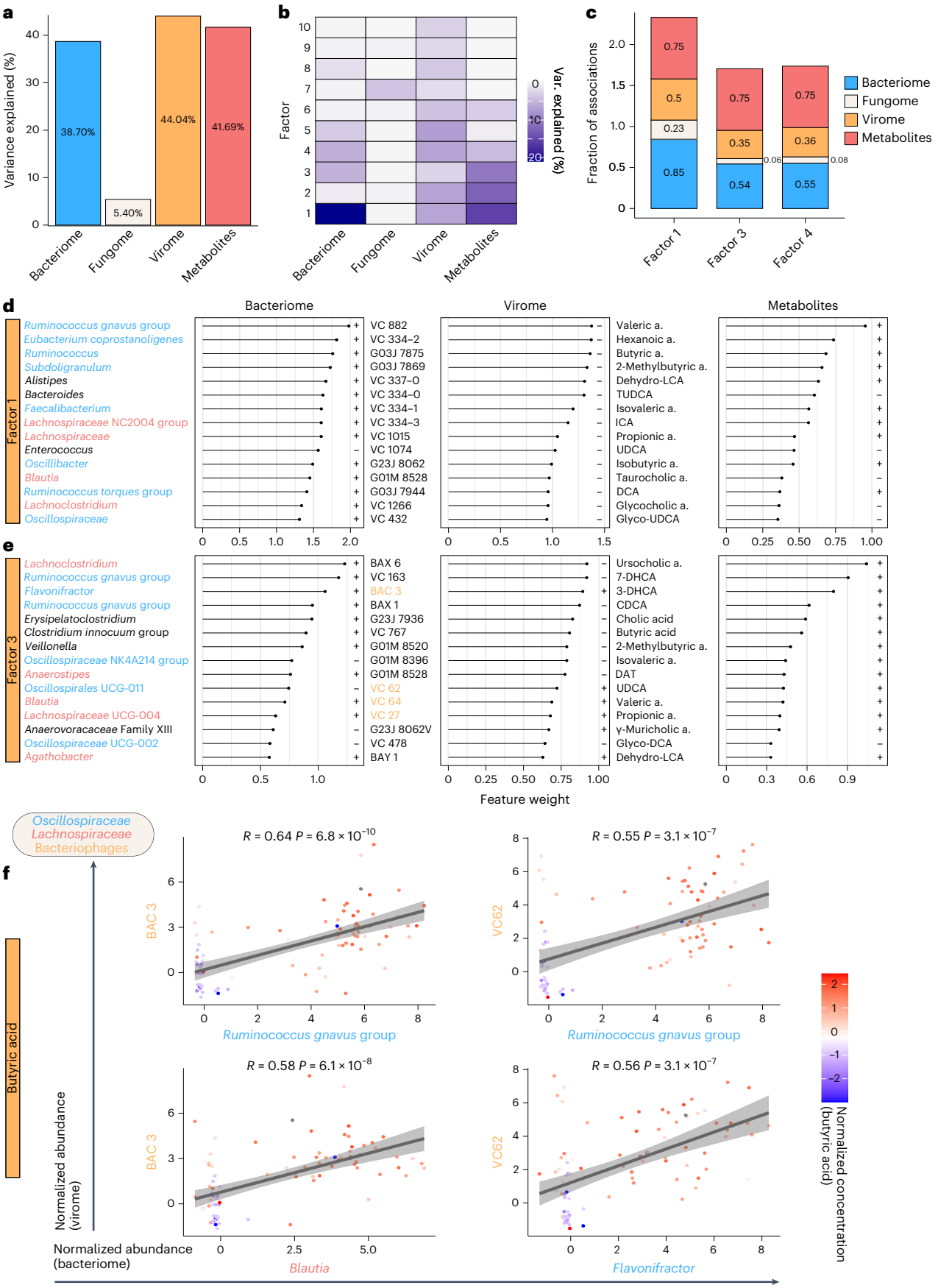

https://doi.org/10.1038/s43018-023-00669-x

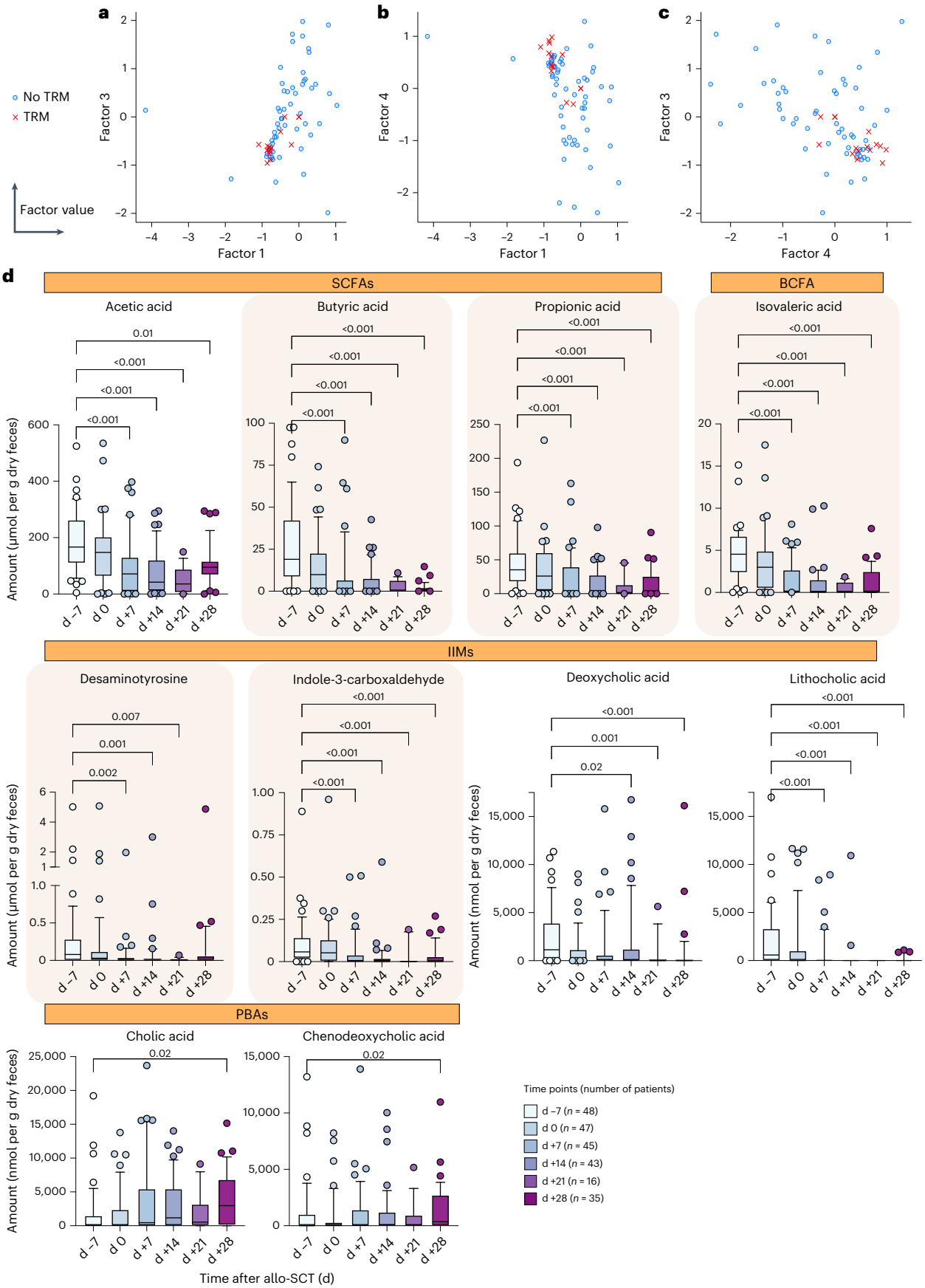

Fig. 4 | MOFA factors are associated with outcome, and levels of MOFA-identified IMMs decline progressively after allo-SCT. a, Factor values of factor 3 plotted against values of factor 1 (averaged across days +7–21). Points are colored and shaped according to the clinical outcome TRM. Blue circles, no TRM at 2-year follow-up (n = 58 patients); red crosses, deceased due to TRM at 2-year follow-up (n = 15 patients). **b**, As in **a**, but factor values of factor 4 are plotted against values of factor 1. **c**, As in **a**, but factor values of factor 3 are plotted against values of factor 4. **d**, Levels of intestinal microbiota-derived metabolites at time points relative to allo-SCT (day 0) in µmol or nmol (BAs) per g of dried stool samples measured by targeted MS. Metabolites identified as high-weight features in MOFA factors 1 and 3 are shown. Shown are (1) SCFAs, (2) a BCFA, (3) IIMs and PBAs. The number of patients at each time point is indicated at the bottom. Metabolites that comprise the IMM-RI are highlighted with background shading. Significance was determined by the two-sided Kruskal–Wallis test and corrected for multiple testing by Dunn's test of data at all time points against baseline (day −7). In the box plots, the box ranges from the 25th to the 75th percentile. The line in the middle of the box is plotted at the median. The whiskers are drawn down to the 10th percentile and up to the 90th percentile. Points below and above the whiskers are drawn as individual points. Points indicate individual patient stool samples sampled at the specified time points.

defined by MOFA factors 1 and 3 was associated with outcome. We observed that low factor 1 and 3 or either together with high factor 4 identified individual patients that were deceased due to transplant-related mortality (TRM) at a 2-year follow-up (Fig. 4a–c). Once we determined optimal factor value cut points via the Youden index, we noted that increased factors 1 and 3 or decreased factor 4 were significantly correlated with overall survival (OS) by the log-rank test (Supplementary Table 3).

The mechanism that links bacterial diversity with outcome is not well understood. We hypothesized that this may be in part due to a depletion of beneficial metabolites, and therefore we assessed intestinal metabolite levels sequentially starting at day −7 before allo-SCT (baseline). In addition to MOFA-identified metabolites, we included BAs that have been previously described to attenuate GvHD (UDCA[26], TUDCA[27]) or to regulate IFN-I responses (DCA, LCA)[28] in our analysis. IMM levels declined progressively after allo-SCT: at day +21, their median intestinal concentration was substantially reduced compared to baseline, for example, butyric acid (162-fold reduction), propionic acid (68-fold), isovaleric acid (149-fold), DAT (53-fold) and ICA (475-fold) (Fig. 4d), and likewise for the IIMs DCA (73-fold) and LCA (41-fold). Analogous to metabolite expression profiles (Extended Data Fig. 2c,d), depletion of these IMMs persisted until at least 1 month after allo-SCT. By contrast, at day +28, we observed a significant increase in levels of the PBAs CA (40-fold increase) and CDCA (430-fold) as well as the SBAs TUDCA (313-fold) and UDCA (26-fold) compared to baseline (Extended Data Fig. 5e).

We hypothesized that low levels of IMMs might be deleterious in patients receiving allo-SCT. Considering (1) the shared microbial biosynthesis pathways for production of different SCFA molecules (for example, regulation of acetate and propionate metabolism via the tricarboxylic acid cycle[29]) and (2) the detection of taxa associated with both SCFAs and BCFAs (Extended Data Fig. 4) but (3) the distinct pathways involved in SCFA, tryptophan derivative and DAT synthesis, we developed the IMM risk index (IMM-RI) to associate metabolites with clinical outcomes. We established the IMM-RI by compounding intestinal levels of the SCFAs butyric and propionic acid, the BCFA isovaleric acid and the IIMs DAT and ICA. These MOFA-identified metabolites were selected based on significant associations with OS (Supplementary Table 4) or, in the case of butyric acid, based on prior studies reporting a negative correlation with adverse outcomes in allo-SCT[14].

First, we confirmed that patients with above-median bacterial diversity had significantly higher OS, less TRM and reduced incidence of GI-GvHD (Fig. 5a and Extended Data Fig. 6a–c) at a follow-up of 2 years. This established that observations in our cohort were comparable to those of other international cohorts[7]. By contrast, neither fungal nor viral diversity correlated with clinical outcome.

In the Kaplan–Meier analysis, the IMM-RI effectively characterized 2-year OS, with 89.5% (standard error, 7%) survival in the low-risk group compared to 47.6% (standard error, 9%) survival in the high-risk group (hazard ratio, 6.2%; 95% confidence interval (CI), 1.4–26.9%; Fig. 5b and Supplementary Table 3). To our surprise, the IMM-RI was significantly associated with relapse: the cumulative incidence of relapse was elevated in the IMM-RI high-risk group, taking into account TRM as the competing risk (Fig. 5c). TRM was also independently correlated with the IMM-RI. Cumulative incidence of GI-GvHD was elevated in the IMM-RI high-risk group, with death as the competing risk (Fig. 5d). With respect to all-cause mortality, the IMM-RI demonstrated an area under the curve of 0.766 (95% CI, 0.634–0.897; Fig. 5e), with a negative predictive value of 0.895 and a positive predictive value of 0.516. All corresponding hazard ratios are reported in Supplementary Table 3.

Patients with low-risk IMM-RI had significantly higher factor 1 and 3 values (Fig. 5f), suggesting an association between these two functional microbiome readouts.

SCFA-synthesis pathways are abundant in IMM-RI low-risk patients

To divulge the microbial pathways that enabled IMM-RI low-risk patients to sustain IMM production during the peri-engraftment period, we performed whole shotgun metagenomic sequencing in a

Fig. 5 | An IMM-RI is associated with OS, relapse, TRM and GvHD. a, Two-year OS after day +21, stratified according to bacterial α-diversity. The mean α-diversity of patient samples at days +7–21 was calculated, and patients were stratified into high- and low-diversity groups, defined as above or below the center-specific median inverse Simpson's diversity index. There were 18 deaths among 35 patients in the low-diversity group (estimated mean survival time, 470 d (95% CI, 382–557 d)) and six deaths among 33 patients in the high-diversity group (estimated mean survival time, 658 d (95% CI, 599–716 d)). The number of patients at risk after 0, 200, 400 and 600 d after day +21 is indicated. Analysis was performed with the Kaplan–Meier estimator; significance was determined according to the log-rank test. All hazard ratios are reported in Supplementary Table 3. **b**, OS after a follow-up of 2 years after day +21, stratified according to high-risk and low-risk IMM-RI, which considers optimal intestinal levels at days +7–21 of the metabolites indicated in the text box. Optimized thresholds for metabolite concentrations were determined using the Youden index (Supplementary Table 9). Analysis was performed with the Kaplan–Meier estimator; significance was determined by the log-rank test. **c**, Cumulative incidence of relapse and TRM after 2 years after day +21 in a competing risk analysis, stratified according to high-risk and low-risk IMM-RI. Cumulative incidence functions between groups were tested for equality using Gray's test; the P value is indicated. **d**, Cumulative incidence of GvHD and its competing risk death after 2 years after day +21 in a competing risk analysis, stratified according to high-risk and low-risk IMM-RI. Statistics are as in **c**. **e**, Receiver operating characteristic curve indicating sensitivity and specificity for the IMM-RI to predict all-cause mortality. The area under the curve (AUC) is indicated; positive predictive value = 0.516 and negative predictive value = 0.895. **f**, Box plots of factor values for factors 1 and 3 (averaged across days +7–21) in IMM-RI low- versus high-risk patients. The center line corresponds to the median; the box ranges from the 25th to the 75th percentile. Whisker length corresponds to the largest or lowest data point that does not exceed the 75th or 25th percentile ±1.5-fold interquartile range (IQR). Blue, low IMM-RI (n = 19 patients); red, high IMM-RI (n = 30 patients). Statistics were determined by two-tailed Mann–Whitney U-test and corrected for multiple testing by the FDR approach.

https://doi.org/10.1038/s43018-023-00669-x

subset of IMM-RI low- and high-risk patients. The most significant and differentially abundant microbial pathways involved the degradation of 4-aminobutanoate to butyric acid (PWY-5022), the biosynthesis of thiamine diphosphate (vitamin B1, PWY-7282), starch degradation III (PWY-6731) and the degradation of *N*-acetylneuraminate to acetic acid or ethanol (P441-PWY) as well as histidine degradation (PWY-5030 and HISDEG-PWY) (Fig. 6a,b). These and related pathways were detected predominantly in *Flavonifractor plautii* of the *Oscillospiraceae* family, matching MOFA-identified bacteria (Extended Data Fig. 7a).

In IMM-RI low-risk patients, we identified an increased abundance of metabolic pathways involved in starch and amino acid (including proteinogenic and non-proteinogenic amino acids) degradation (Fig. 6c and Extended Data Fig. 7b). Via the pathway PWY-5022, bacteria can degrade the non-proteinogenic amino acid 4-aminobutanoate (GABA), an inhibitory neurotransmitter, to butyric acid. As we noted that various pathways related to fermentation were highly differentially abundant (Fig. 6b), we combined these into a superclass of fermentation, which was significantly increased in IMM-RI low-risk patients (Fig. 6d). Because SCFAs are derived from the fermentation of dietary fibers, complex carbohydrates including starches or amino acids, we specifically analyzed a superclass of SCFA synthesis, which includes biosynthesis pathways of acetic, butyric and propionic acid (Fig. 6e and Supplementary Table 5). We observed an increased abundance of the SCFA superclass in IMM-RI low-risk patients, which corresponded

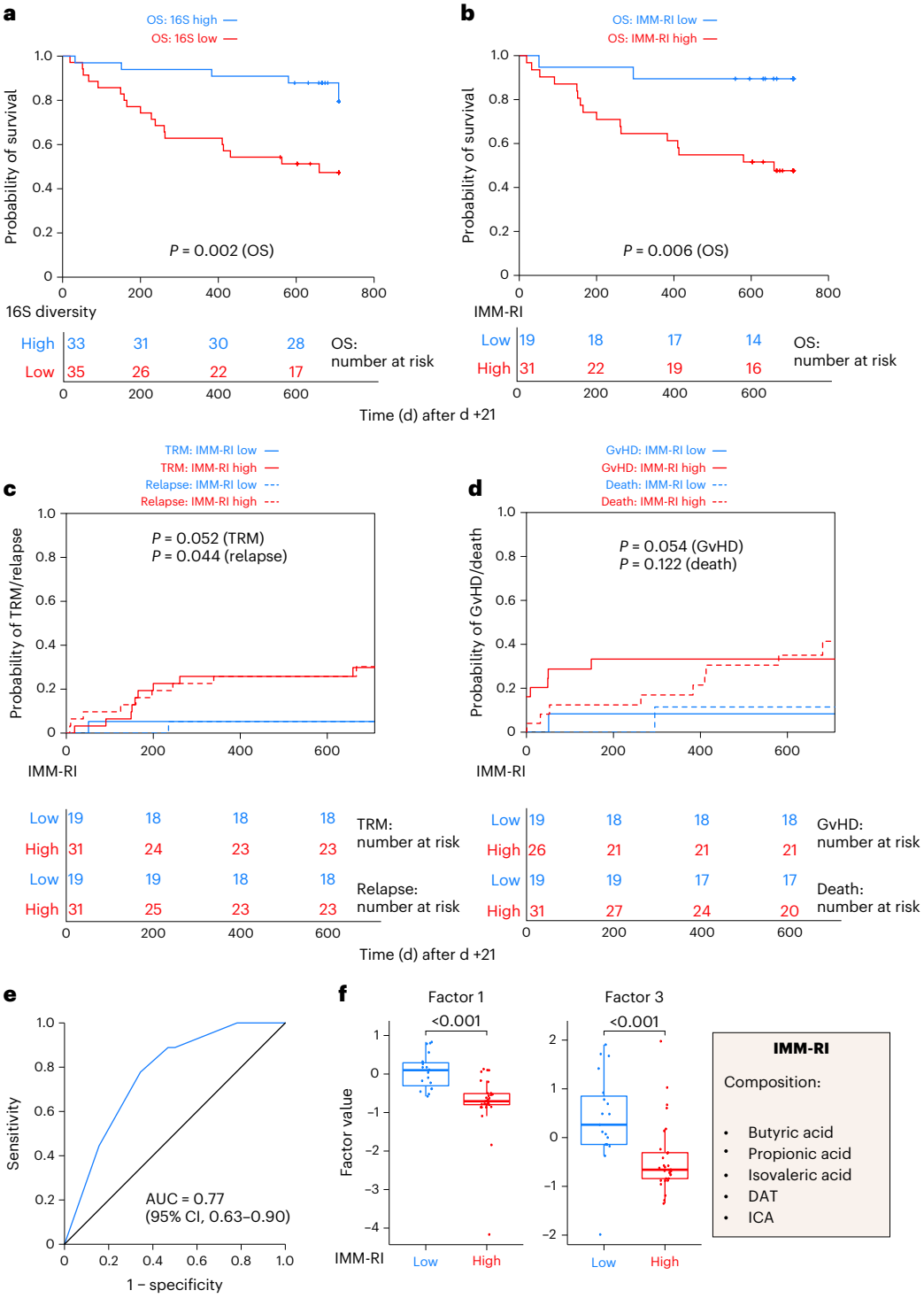

https://doi.org/10.1038/s43018-023-00669-x

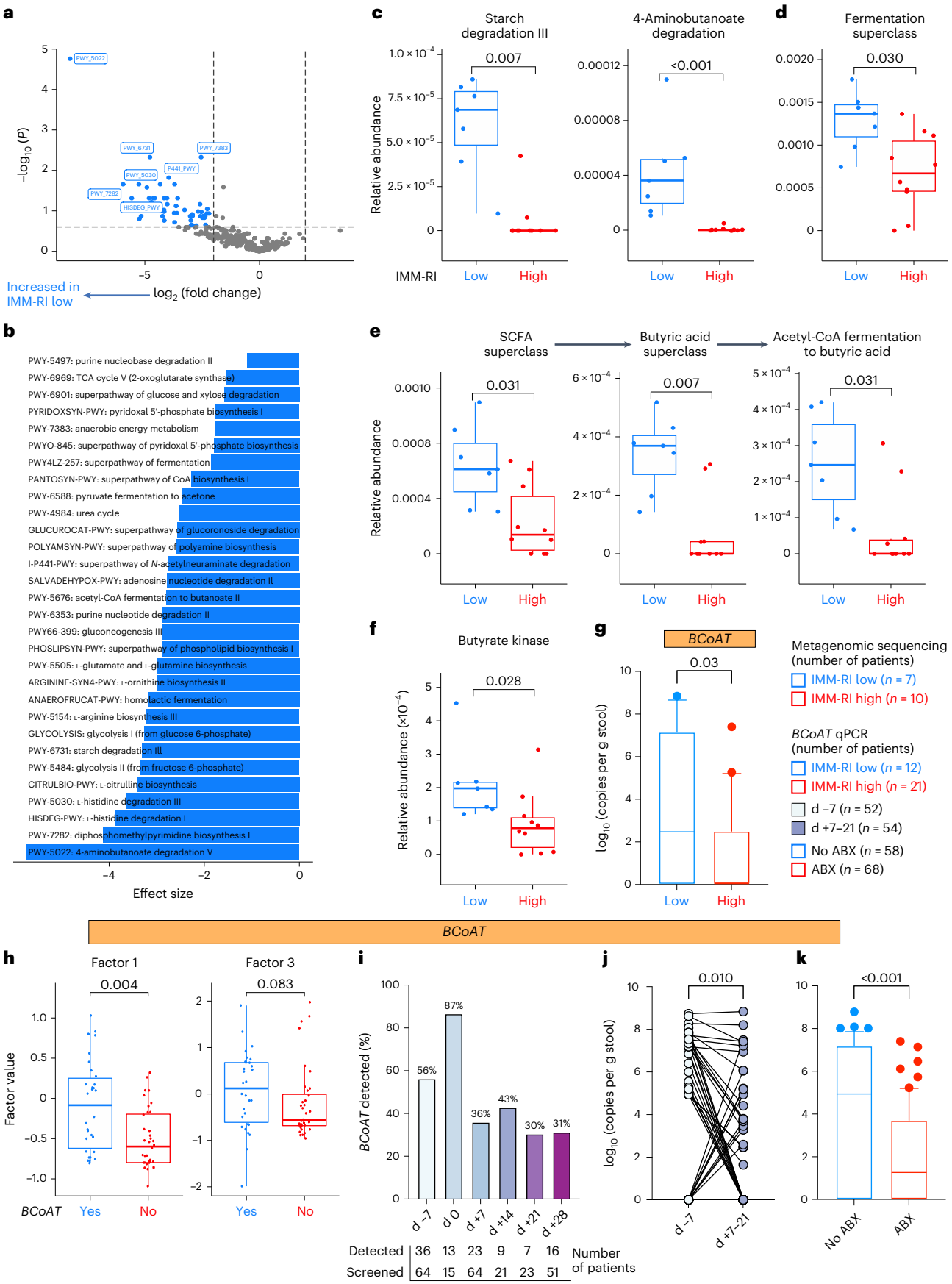

https://doi.org/10.1038/s43018-023-00669-x

Fig. 6 | Microbial SCFA- and butyric acid-biosynthesis pathways are more abundant in IMM-RI low-risk patients. a, Volcano plot of differentially abundant microbial pathways identified by metagenomic sequencing in IMM-RI low- versus high-risk patients. Blue dots indicate pathways that are significantly more abundant in IMM-RI low-risk patients; their BioCyc ID is shown. The *x* axis shows fold change ($\log_2$); the *y* axis shows *P* values ($-\log_{10}$) adjusted for multiple comparisons with the Benjamini–Hochberg procedure. **b**, Waterfall plot of differentially abundant microbial pathways in IMM-RI low- versus high-risk patients identified with MaAsLin 2. Only features in the IMM-RI low-risk group were significant after applying abundance and *P*-value cutoffs ($P \leq 0.01$) and are shown. BioCyc IDs and MetaCyc pathway names are indicated. The *x* axis denotes the effect size. TCA, tricarboxylic acid cycle. **c**, Relative abundance of the specified MetaCyc pathways in IMM-RI low- versus high-risk patients. **d**, Summarized relative abundances within the fermentation superclass in IMM-RI low- versus high-risk patients. **e**, Summarized relative abundances within the SCFA and butyric acid superclasses and the indicated MetaCyc pathway in IMM-RI low- versus high-risk patients. **f**, Relative abundance of butyrate kinase in IMM-RI low- versus high-risk patients. **g**, *BCoAT* copy numbers (in $\log_{10}$) per g of stool quantified by qPCR according to low- versus high-risk IMM-RI. **h**, Factor values for factors 1 and 3 (averaged across days +7–21) according to whether *BCoAT* copies were detected by qPCR ('yes') or not detectable ('no'). Blue, detected ($n = 30$ patients); red, not detectable ($n = 36$ patients). **i**, Detection of *BCoAT* copies in patients according to time point. Bar plots show percentage; exact values are provided. The numbers of patients screened versus those in which *BCoAT* was detected is indicated below. **j**, *BCoAT* copy numbers (in $\log_{10}$) in paired patient samples at day −7 compared to the peri-engraftment period (samples averaged across days +7–21). **k**, *BCoAT* copy numbers in paired patients samples before ('no ABX') and after exposure to antibiotics ('ABX'). For all box plots, the box ranges from the 25th to the 75th percentile. The line in the middle of the box is plotted at the median. The whiskers are drawn down to the minimum and up to the maximum. Samples outside the 1.5-fold IQR were regarded as outliers. In **h**, whisker length corresponds to the largest or lowest data point that does not exceed the 75th or 25th percentile ±1.5-fold IQR. Individual patient samples are plotted as a point superimposed on the graph. The number of patients in each group is indicated in **g**, right. Statistics: **c**–**e**, one-sided Wilcoxon test and Benjamini–Hochberg correction for multiple testing; **g**, two-sided Mann–Whitney test; **h**, two-tailed Mann–Whitney *U*-test and FDR correction for multiple testing; **j**, two-sided Wilcoxon test; **k**, two-sided Mann–Whitney test.

to a significant increase in butyric acid abundance and a nonsignificant elevation in acetic and propionic acid-biosynthesis pathways (Fig. 6e and Extended Data Fig. 7c).

Aside from SCFA biosynthesis, we detected a higher abundance of pathways involved in amino acid synthesis (including essential and non-essential amino acids), amino acid degradation (histidine), purine nucleotide degradation (including adenosine and guanosine) and vitamin B synthesis (Extended Data Fig. 7b) in IMM-RI low-risk patients. Degradation of L-histidine via the HISDEG-PWY pathway can lead to production of the metabolite imidazole propionate, which was shown to modulate host inflammation and metabolism[30]. Purine metabolism was recently linked to efficacy of immunotherapy[31], while vitamin B synthesis[32] was associated with protection from colitis. Genes involved in the conversion of PBAs to SBAs were not differentially abundant.

Butyric acid is synthesized via the intermediates acetyl-CoA and butyryl-CoA. Synthesis is completed with the enzymes butyrate kinase (EC 2.7.2.7) or butyryl-CoA:acetate CoA-transferase (EC 2.8.3.8, encoded by the gene *BCoAT*)[33]. Both genes were more abundant in IMM-RI low-risk patients (Fig. 6f,g). We quantified *BCoAT* copy numbers by quantitative PCR analysis (qPCR). Patients in whom *BCoAT* was detected had a significantly higher factor 1 value (Fig. 6h). The detection of *BCoAT* was reduced in the peri-engraftment period (Fig. 6i), and copy numbers declined significantly in paired patient samples after day −7 (Fig. 6j). We observed significantly reduced *BCoAT* copy numbers in patients exposed to antibiotics (Fig. 6k), confirming our previous findings that antibiotics are an independent risk factor for low *BCoAT* copy numbers[34].

Bacteriophages encode the butyric acid-synthesis gene *BCoAT*

Bacteriophages can modulate bacterial metabolism via AMGs[21], which are activated when phages infect their hosts and then augment or redirect specific metabolic pathways within them[20,21]. To identify phage-coded AMGs, we mined our viral metagenomic sequencing dataset for the microbial pathways and genes identified above. We detected whole-length *BCoAT* (1.34 kb) and a 450-bp fragment of *BCoAT* encoded in two individual bacteriophage contigs with almost complete phage genome length: VC-2 (90,756 bp) and VC-1 (77,772 bp). Phylogenetic analysis showed a close evolutionary relationship of bacteriophage-coded *BCoAT* to its homologs from *Oscillospiraceae*, indicating that this gene may have been acquired from this bacterial family (Fig. 7a). In addition, we discovered *BCoAT* in a *Myoviridae* sp. bacteriophage (GenBank ID DAV55430.1) identified in another cohort of human metagenomic samples including those from the Human Microbiome Project[35], indicating that the two *BCoAT*-coding phages identified in this study are unlikely to be an assembly artifact.

We aligned *BCoAT* encoded in VC-2 against a closely related bacterial reference sequence from *Lawsonibacter* (a species within *Oscillospiraceae*) and observed a close match in sequence identity for both *BCoAT* and the adjacent gene encoding a DEAD-box helicase (Fig. 7b and Extended Data Fig. 8a), which in bacteria are involved in ribosome biogenesis and translation initiation[36]. Meanwhile, VC-1, which encoded a part of the *BCoAT* gene, aligned with *Pseudoflavonifractor*, another member of *Oscillospiraceae* (Extended Data Fig. 8b).

Genomic assembly and annotation characterized VC-2 and VC-1 as temperate bacteriophages, evident by the presence of genes for integration, excision and packaging (Fig. 7c). Phage AMGs are frequently located within auxiliary gene cassettes and are separated by structural and nucleotide metabolism cassettes[20,37]. The organization of *BCoAT* in the genomes of VC-2 and VC-1 was consistent with this: the tail (structural) gene cassettes were clustered together but located separately from the *BCoAT* AMG.

Patients who harbored VC-2 and VC-1 had significantly elevated factor 1 values (Extended Data Fig. 8c,d). We observed that VC-2 and VC-1 were more abundant and more likely to be detected in IMM-RI low-risk

Fig. 7 | Detection of the *BCoAT* AMG encoded in VC-1 and VC-2 bacteriophages. **a**, Circle phylogenetic tree of bacteriophage-coded *BCoAT* compared against bacterial reference sequences. *BCoAT* was detected in two unique viral contigs, VC-1 and VC-2, as well as in *a Myoviridae* sp. bacteriophage. Bacterial taxonomy is indicated at the bottom left. Branch length is indicated in the center. **b**, Gene-alignment plot of the VC-2-coded *BCoAT* against a closely related reference sequence in *Lawsonibacter* (an *Oscillospiraceae* family member). Dark gray shading indicates identity overlap in percent. A detailed plot is provided in Extended Data Fig. 8. **c**, Circle diagram of the VC-1 and VC-2 genomes by viral genome assembly. Genomic regions and their functions are indicated at the bottom. The *BCoAT* AMG is shown in red. **d**, From left to right, relative abundance of VC-1 according to low- versus high-risk IMM-RI, detection of VC-1 in patients according to time point and relative abundance of VC-1 in paired patients samples before ('no ABX') and after exposure to antibiotics ('ABX'). Bar plots show percentage; exact values are provided. The numbers of patients screened and in whom VC-1 was detected is indicated below. In the box plots, the box ranges from the 10th to the 90th percentile. The line in the middle of the box is plotted at the median. Whiskers are drawn down to the minimum and up to the maximum. Samples outside the 1.5-fold IQR were regarded as outliers. High IMM-RI, $n = 72$ samples; low IMM-RI, $n = 63$ samples. 'No ABX', $n = 40$ patients; 'ABX', $n = 39$ patients. Significance was determined by two-tailed Mann–Whitney test. **e**, As in **c** for VC-2. **f**, Correlation of relative abundance of VC-1 or VC-2 with intestinal butyric acid levels (in µmol per g of dry feces) was determined by Spearman's correlation. Axis is on a log scale. *R* and *P* values are indicated in each plot. Number of pairs, 130 samples.

https://doi.org/10.1038/s43018-023-00669-x

patients than in high-risk patients (Fig. 7d,e and Extended Data Fig. 8e,f). Despite their low relative abundance, we detected VC-2 and VC-1 in more than 60% and 80% of patients across both centers at day −7, respectively, but detection declined progressively during the peri-engraftment period. Exposure to antibiotics resulted in a significant decrease in the relative abundance of VC-2 and VC-1. The abundance of both bacteriophages was moderately correlated with intestinal butyric acid levels as assessed by Spearman's correlation (Fig. 7f).

Onset of GI-GvHD and exposure to antibiotics impact IIMs

Clinical events during the peri-engraftment period, such as onset of GI-GvHD and initiation of broad-spectrum antibiotics, have been shown to compound the detrimental effect of allo-SCT on the bacterial microbiome[6,7,38] and may impact intestinal IIMs.

We performed a subgroup analysis in patients with clinical diagnosis of GI-GvHD of any severity matched by time point to a control group of allo-SCT patients without GvHD. In patients with GI-GvHD,

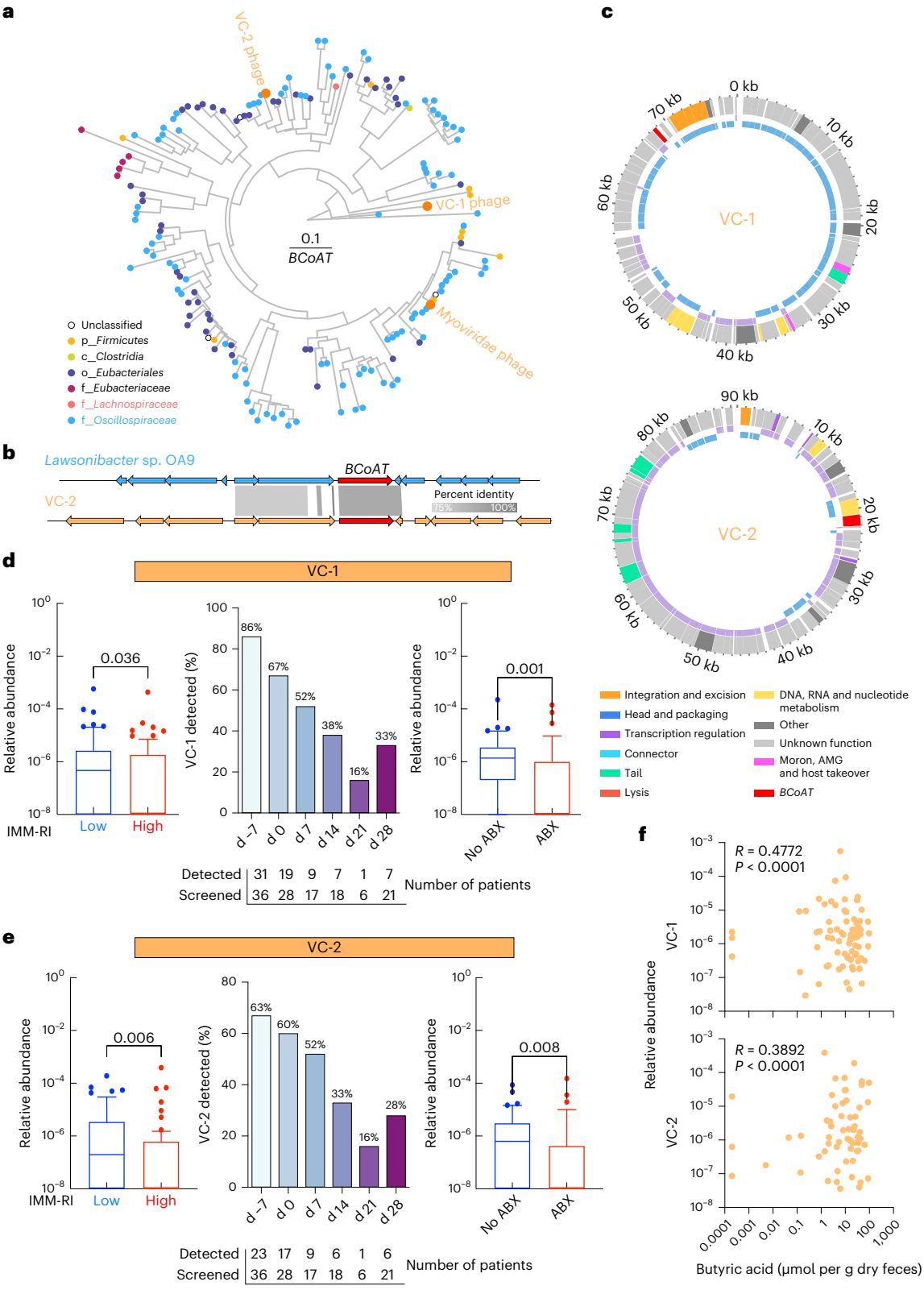

https://doi.org/10.1038/s43018-023-00669-x

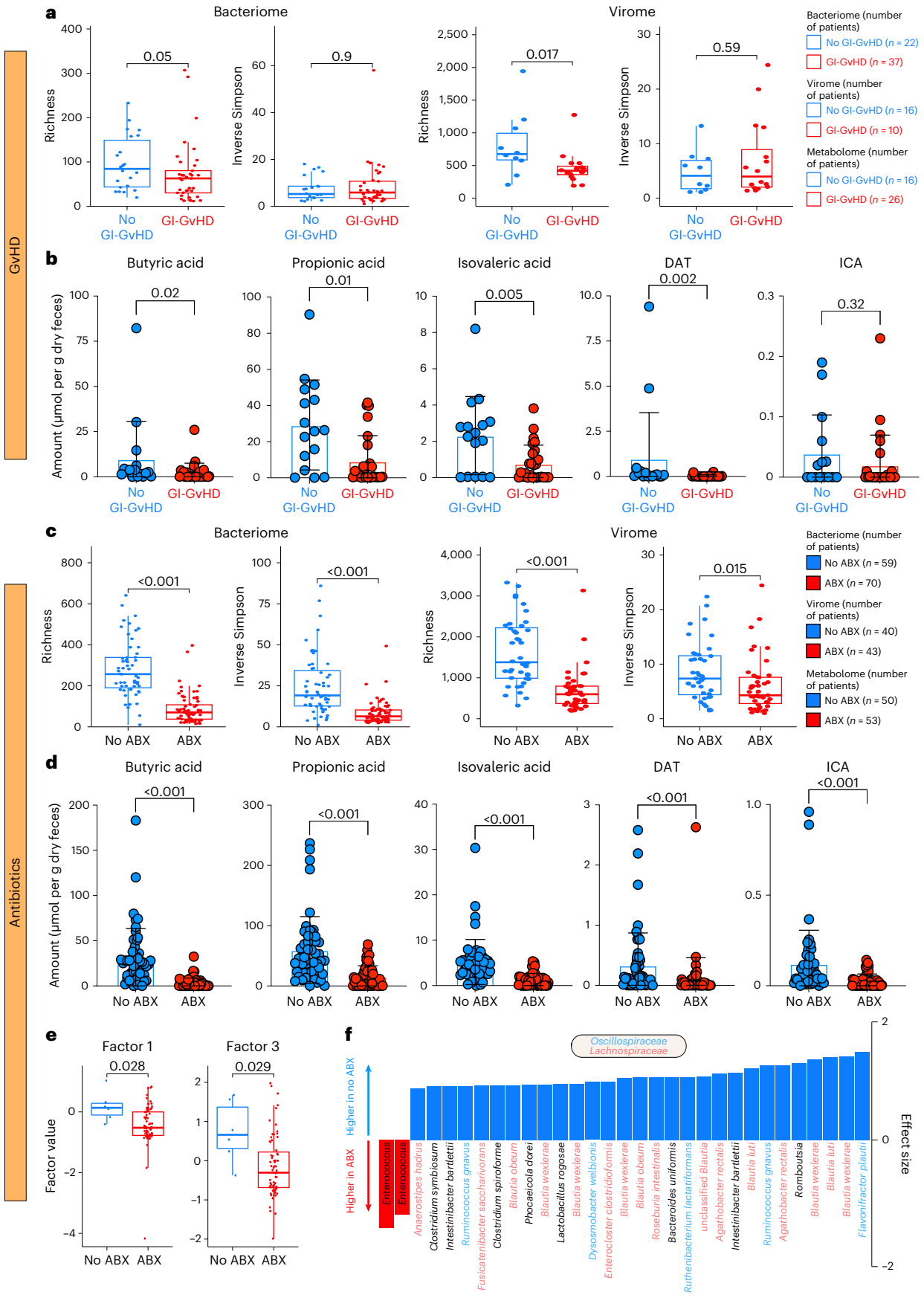

Fig. 8 | Onset of GI-GvHD and initiation of antibiotics deplete IMMs. **a**, Intestinal bacterial and viral α-diversity (richness, inverse Simpson's diversity index), stratified by patients diagnosed with GI-GvHD (GI-GvHD) versus control patients receiving allo-SCT (no GI-GvHD). Significance was determined by two-tailed Wilcoxon rank-sum test and adjusted for multiple comparisons with the Benjamini–Hochberg procedure. The box ranges from the 25th to the 75th percentile. The line in the middle of the box is plotted at the median. Whiskers are drawn down to the minimum and up to the maximum. Samples outside the 1.5-fold IQR were regarded as outliers. Each individual patient is plotted as a point superimposed on the graph. The number of patients per group is indicated on the right. **b**, Levels of IMM-RI metabolites (in µmol per g of dry stool) stratified by patients diagnosed with GI-GvHD versus control patients receiving allo-SCT. Significance was determined by two-tailed Mann–Whitney test. In the scatter dot plots, the box is plotted at the mean. Error bars indicate s.d. Each individual patient is plotted as a point superimposed on the graph. The number of patients per group is indicated in **a**, right. **c**, Intestinal bacterial and viral α-diversity as in a in paired patient samples according to antibiotic status: 'no ABX' (blue) or 'ABX' (red). Once a patient was treated with antibiotics, the current and all subsequent samples were classified as 'ABX'. Significance was determined by two-tailed Wilcoxon rank-sum test and adjusted for multiple comparisons with the Benjamini–Hochberg procedure. Box plots are as described in **a**. The number of patients per group is indicated on the right. **d**, IMM-RI metabolite levels in patient samples according to antibiotic status as in **e**. Significance was determined by two-tailed Wilcoxon matched-pair signed-rank test. Scatter dot plots are as described in **b**. **e**, Box plots of factor values for factors 1 and 3 according to antibiotic status (averaged across days +7–21). Box plots are as described in **a**, except that whisker length corresponds to the largest or lowest data point that does not exceed the 75th or 25th percentile ±1.5-fold IQR. Blue, 'no ABX' ($n = 6$ patients); red, 'ABX' ($n = 67$ patients). Significance was determined by two-tailed Mann–Whitney *U*-test and corrected for multiple testing by the FDR approach. **f**, Waterfall plot of differentially abundant bacterial taxa in patient samples according to antibiotic status. Only significant taxa with a P-value cutoff ($P \leq 0.01$) are shown. Blue bars indicate species that are more abundant in patients not exposed to antibiotics; red indicates species that are more abundant after ABX. The *x* axis denotes the effect size.

we observed a trend toward lower bacterial α-diversity and load as well as a significant decline in viral richness compared to controls (Fig. 8a and Extended Data Fig. 9a). We did not observe any differences in fungal diversity or load (Extended Data Fig. 9a,b). β-diversity analysis showed significantly distinct clustering of bacterial and viral but not fungal communities in patients with GI-GvHD compared to controls (Extended Data Fig. 9c).

Patients with GI-GvHD presented with significantly lower levels of IMM-RI metabolites (Fig. 8b). Only ICA showed a nonsignificant reduction. Levels of other IMMs such as acetic, valeric, 2-methylbutyric and isobutyric acid were also significantly reduced (Extended Data Fig. 9d). Of the BAs, only LCA levels were significantly decreased in patients with GI-GvHD compared to controls, while CA, CDCA, UDCA and TUDCA levels were comparable between both groups (Extended Data Fig. 9d).

During the course of their hospital stay, 100% of MUC and 94% of REG patients were started on broad-spectrum antibiotics (Supplementary Table 6) according to center-specific standards (Supplementary Table 2). We longitudinally analyzed matched patient samples before and after ABX. ABX resulted in a significant decrease of bacterial α-diversity and load as well as viral richness (Fig. 8c and Extended Data Fig. 10a). Fungal diversity or load was not impacted by ABX (Extended Data Fig. 10a,b). By β-diversity analysis, we observed that ABX resulted in major and significant changes to bacterial and viral but not fungal community compositions (Extended Data Fig. 10c).

ABX drastically affected the metabolites comprising the IMM-RI and resulted in their depletion to levels approaching the lower limit of detection (Fig. 8d). Other IMMs were also significantly diminished (Extended Data Fig. 10d). Likewise, MOFA factor 1 and 3 values declined significantly after ABX (Fig. 8e). By contrast, we observed that the BAs CA, UDCA and TUDCA were significantly increased in patients after ABX (Extended Data Fig. 10d). At species level, we observed that antibiotic-exposed patients had a higher abundance of *Enterococcus* (Fig. 8f) but a decrease in species predominantly within the *Lachnospiraceae* and *Oscillospiraceae* families, many of which corresponded to high-weight bacterial features identified by MOFA, for example, *Blautia wexlerae* or *F. plautii*.

Discussion

We identified a functional microbiome signature composed of bacteria within the *Oscillospiraceae* and *Lachnospiraceae* families and their associated bacteriophages. This signature was linked to the production of intestinal SCFAs, BCFAs and IIMs, which were associated with increased OS, reduced TRM and less relapse after allo-SCT. Recently, defective oxygen utilization in IECs was linked to the loss of intestinal hypoxia during GvHD[39]. This supports our finding that the obligate anaerobic *Oscillospiraceae* and *Lachnospiraceae* families were associated with IMMs, which together may exert local, protective effects on IECs, and that these consortia and their metabolites are depleted during GvHD when a shift to an aerotolerant microbiome occurs.

MOFA-identified bacteria included *Roseburia*, which are known butyrate producers and affect colonic motility, maintain immunity and exert anti-inflammatory properties[40]. *F. plautii*, a species linked to T_{reg} induction in mice after oral administration[41], comprised factor 3 and was associated with butyric acid production via *BCoAT*. We characterized bacteriophages that were tightly correlated with their *Oscillospiraceae* or *Lachnospiraceae* hosts, and, when both were highly co-abundant, we observed high-level expression of intestinal IMMs. This association between the bacteriome, the virome and metabolites may suggest an important role for bacteriophages in synthetic consortia engineered to produce metabolites. However, it remains to be determined through in vitro follow-up studies whether bacteriophages are essential for metabolite production or whether they simply coexist with their respective hosts.

Our viral metagenomic sequencing pipeline, which was optimized for non-targeted DNA sequencing from isolated VLPs and uses large sample masses to avoid bias associated with whole-genome amplification, allowed us to observe a high abundance of bacteriophages in patients, which declined along with intestinal bacterial diversity after allo-SCT. Our results partially align with a study of the intestinal virome in 44 patients after allo-SCT, which found an increase in eukaryotic viruses and a decrease in bacteriophage richness[24]. Although there were no major alterations in the intestinal eukaryotic virome and we detected human DNA viruses such as *Poxviridae* and *Papillomaviridae*, we acknowledge that our viral sequencing pipeline was not enriched for RNA virus detection. However, given that bacteria make up more than 50% of total solids in human feces[42], our findings suggest that virome alterations during allo-SCT occur at the level of bacteriophages, which shift in response to factors affecting their host bacteria. This is consistent with a recent MOFA in patients with sepsis at the intensive care unit, which showed that bacteria and their bacteriophages covaried in factors driven by antibiotic perturbation[43].

Fungal diversity and load by ITS sequencing remained stable during allo-SCT and did not decline in patients with GI-GvHD[44]. The low MOFA-explained variance in the fungome suggested that MOFA considered most of the variations within this dataset to be random and not driven by specific feature-covariation patterns that might represent distinct biological states. By contrast, culture-based studies have identified a subset of patients in which *Candida parapsilosis* complex species were correlated with worse OS and higher TRM[44] and found that colonization by *Candida* spp. was associated with more severe GvHD[45]. For associations with clinical outcome, traditional culture-based methods remain the standard.

Microbiota-derived metabolites have been shown to protect from GvHD in animal models[11–13,46]. Previous studies in patients receiving allo-SCT have been cross-sectional and focused on metabolites in the blood[15,47]. An untargeted MS-based screening of metabolites in the serum of allo-SCT recipients and donors in French transplant centers found that, at the onset of GvHD, levels of tryptophan derivatives and other aryl hydrocarbon receptor ligands were decreased[15]. In line with this, we observed a trend toward reduction of the tryptophan derivative ICA in patients with GI-GvHD and a significant reduction in patients receiving allo-SCT during the peri-engraftment period. In the same study, levels of the serum SBAs UDCA and TUDCA were increased in patients with acute GvHD. We observed a significant increase in intestinal UDCA and TUDCA at late time points after allo-SCT and in patients exposed to antibiotics but noted no differences in patients with GI-GvHD compared to controls. The use of peroral UDCA to prevent hepatic complications and severe acute GvHD in patients receiving allo-SCT[26] may explain elevated levels of fecal UDCA at late time points (Supplementary Table 2).

Aside from SCFAs, we observed that allo-SCT impacted expression of several intestinal metabolites that were not previously described in the human allo-SCT setting, such as DAT[48], ICA[12], LCA[49] and DCA[50]. These metabolites, which we refer to as IIMs, are potent activators of IFN-I signaling, which can positively or negatively modulate GvHD, depending on the timing of IFN-I activation[51]. DAT, also known as phloretic acid, a byproduct of flavin degradation, can enhance IFN-I responses and antiviral activity in murine respiratory influenza infection[48]. We detected ICA, which has been shown to target aryl hydrocarbon receptors and protect mice from metabolic syndrome[52] as well as GvHD[12] via IFN-I[12]. We measured levels of DCA, which has been shown to restrict alphavirus infection in mice via IFN-I[50]. The SBA LCA was decreased in patients with GI-GvHD, and two recent studies have associated SBAs with T_{reg} differentiation[13,53], which plays a vital role in restraining GI-GvHD. Recently, intestinal levels of DAT together with DCA, LCA and other SBAs were compounded in a 'microbiome metabolic profile' and associated with outcome in critically ill patients with coronavirus disease 2019 (COVID-19)[54]. In our study, intestinal levels of IMM-RI metabolites declined progressively after allo-SCT, and these changes persisted until at least 1 month after allo-SCT. In patients with GI-GvHD, IMM levels were particularly low, but further conclusions are limited by the number of patients in these two subgroups ($n = 26$ and $n = 16$ for GI-GvHD and controls, respectively).

The IMM-RI predicted OS and was independently associated with reduction of TRM and relapse rate. While our non-interventional study is limited to associating microbiome signatures and metabolites with clinical outcome after allo-SCT, there are plausible mechanisms by which the metabolites that constitute the IMM-RI might impact outcomes. A decrease in TRM may reflect the observed reduction in the incidence and severity of GvHD and aligns with the reduction in butyric acid levels reported in patients with severe GI-GvHD[14]. Indeed, T_{reg} cells, which can be activated by metabolites including SCFAs[55], play a crucial role in controlling GvHD[11]. Glucagon-like peptide 2 was shown to reduce GI-GvHD by promoting IEC regeneration but had no effect on the graft-versus-leukemia effect[56]. Therefore, the reduced relapse rate in IMM-RI low-risk patients may be dependent on other metabolites aside from SCFAs, such as IIMs, which could augment IFN-I signaling and invoke the graft-versus-leukemia effect in patients[57]. The effects on both TRM and relapse may be interpreted as a cumulative effect of intestinal metabolites with different underlying modes of action.

Only a few studies have reported an association between the intestinal microbiota and relapse after allo-SCT[58]. As expected, bacterial α-diversity correlated with OS but did not predict relapse rate. However, a low IMM-RI was significantly associated with a reduced relapse rate, considering its competing risk TRM. We detected no significant differences with regard to sex, Hematopoietic Cell Transplantation-Comorbidity Index, disease risk, conditioning intensity, exposure to antibiotics and other parameters between IMM-RI low- and high-risk patients (Supplementary Table 7). Old age correlated with high-risk IMM-RI, which is consistent with age being a risk factor for an increase in biomarkers of acute GI-GvHD[38] and with age-related changes of intestinal microbiota promoting intestinal inflammation and loss of epithelial integrity[59]. However, this association between intestinal IMMs and relapse rate was unexpected, and our study was not a priori designed for this purpose. The number of patients to calculate the IMM-RI was limited ($n = 50$), and few relapse events in this subset (only nine versus one event(s) in high-risk versus low-risk IMM-RI groups, respectively) precluded a multivariable analysis. Therefore, these results should be considered exploratory findings and require confirmation in an international cohort sufficiently powered for multivariate analysis.

Microbial pathways for the biosynthesis of SCFAs were more abundant in IMM-RI low-risk patients, and these results were confirmed for butyric acid biosynthesis by qPCR for *BCoAT*, a gene encoding a key enzyme in the terminal reaction of the acetyl-CoA pathway, the predominant biosynthesis pathway of butyric acid[60]. Strikingly, we identified *BCoAT* encoded in two temperate bacteriophages, VC-2 and VC-1. Environmental stressors, such as antibiotics (for example, mitomycin C[61]), can trigger temperate bacteriophages to change their behavior and initiate a lytic cycle. This cycle results in lysis of host bacteria, release of new phage particles and an increased abundance of host-originated genes, including AMGs, with each subsequent infection. On the other hand, during lysogeny, temperate bacteriophages are stably integrated into the host genome, allowing them to coexist and multiply alongside host cells. Given that bacteriophages do not require metabolism genes, the detection of the *BCoAT* AMG in numerous patients across both centers suggests a selective pressure that provides an advantage in colonizing specific niches. Our data provide intriguing evidence of bacteriophage AMGs in humans, highlighting the potential cooperation of bacteria and their bacteriophages through which they could support metabolite production and potentially benefit patients receiving allo-SCT.

Aside from microbiota, factors relating to host genetics, diet and medication contribute to intestinal metabolite profiles. All MUC patients received in-patient germ-reduced Western pattern fare with a defined macronutrient composition and a goal intake of 2,000 calories per d (Supplementary Table 8). However, associations between diet and metabolites are limited because we did not record individual patient diets.

Antibiotics impact intestinal bacteria[2,34]. Loss of anaerobic commensals and a decrease in intestinal SCFA levels, specifically those of acetate, propionate and butyrate, were associated with severe acute GvHD[14]. Intestinal butyrate and propionate levels were negatively correlated with exposure to antibiotics[62]. By longitudinally tracking patients from before allo-SCT, we were able to analyze in paired patient samples how initial exposure to antibiotics depleted protective IMMs. However, despite antibiotics' dominant effect on the microbiome, other factors such as concomitant medication or diet may have changed between sequential samples and could contribute.

Our findings have far-ranging implications that could be important for other T cell-mediated therapies that are influenced by the gut microbiome, such as chimeric antigen receptor T cells or immune checkpoint inhibitors[63,64]. First, administration of IMMs, either by synthetic bacteria–bacteriophage consortia engineered to produce specific metabolites or directly via metabolite formulations, could be explored in clinical trials in patients receiving allo-SCT affected by biomarker-proven intestinal microbiota disruption (for example, IMM-RI high-risk patients) to treat or prevent GvHD and relapse. Second, screening for IMMs in fecal microbiota transplant products could assist in donor–recipient matching, standardization of product quality

and development of a precision fecal microbiota transplant product that may improve response rates. Third, we have previously shown that timing of ABX impacts the intestinal bacteriome[6], and it stands to reason that limiting ABX or altering its timing could be used to modulate intestinal IMM levels and, with it, clinical outcome.

In clinical scenarios, a functional microbiome snapshot via rapid metabolite measurement would be advantageous over a protracted metagenomic approach. Thus, developing in-hospital assays for a specific index with a limited number of metabolites, such as the IMM-RI, appears feasible.

In sum, our research provides a strong rationale for the design of precision bacterial and viral consortia with desired metabolite profiles (IMMs) as a new frontier in microbiome-based therapies aimed at improving clinical outcomes after allo-SCT and potentially other T cell-mediated therapies.

Methods

Study design

This research complies with all relevant ethical regulations. Study protocols were approved by the institutional review boards 'Ethikkommission der TU München' (295/18S) and 'Ethikkommission der Universität Regensburg' (14-47_1-101, 14-101-0047, 21-2521-01).

We report the 2-year follow-up of a prospective, observational, longitudinal, two-centric cohort of patients receiving allo-SCT. We combined microbiome analysis with targeted metabolomics to characterize intestinal bacterial, fungal and viral community composition together with the intestinal metabolome. The bacteriome and fungome were characterized via 16S and ITS1 amplicon sequencing, respectively. For the virome, we first purified VLPs, followed by whole-genome shotgun sequencing[65]. We applied MS for quantification of microbiota-derived metabolites.

Patients were enrolled at the University Hospital of the Technical University of MUC and the University Hospital REG after obtaining informed consent and in accordance with institutional review board-approved study protocols. Patients did not receive financial participant compensation.

Patient characteristics including numbers, age, sex, diagnosis and survival are exhibited in Supplementary Table 1. The study cohort included female and male patients. Sex (biological attribute) was assigned based on electronic patient records. We did not consider sex in the study design and did not perform separate analysis according to sex, as sex did not affect microbiome-predicted outcomes in other cohorts of patients receiving allogeneic stem cell transplantation[7,66]. In REG, ethnicity was determined by self-reporting; all patients identified as 'non-Hispanic or white'.

Samples were collected once a week beginning at day −7 before allo-SCT up until day +35 after allo-SCT or when patients were discharged, whichever occurred later. In the event of occurrence of acute GI-GvHD, patients were sampled then and weekly thereafter until resolution of GI-GvHD or death. Samples were obtained 1–2 d around the specified time points. Stool samples were collected in magiX PB1 microbiome preservation buffer (microBIOMix) or as unprocessed, native samples and transferred to the laboratory within 4 h, where they were stored at −80 °C until further processing.

Graft-versus-host disease

GI-GvHD occurred in 50% of patients, of which 30% developed severe GI-GvHD, defined as GI-GvHD grade 2–4 according to the Glucksberg criteria. At occurrence, patients with GvHD received intravenous corticosteroid therapy. Stool samples of patients with active GI-GvHD were labeled as such and compared to time point-matched samples from patients without GvHD (control patients receiving allo-SCT). When more than one sample per patient was available for GI-GvHD-versus-no-GI-GvHD comparison, the mean metabolite concentration was calculated.

Antibiotics

Patient samples were grouped according to antibiotic status: samples categorized as 'no ABX' had no exposure to antibiotics, but once a patient was started on antibiotics, the first and all subsequent samples were classified as 'ABX'. In addition, all samples were annotated according to concomitant anti-infective prophylaxis (site-specific standards; Supplementary Table 2) as well as antifungal and antiviral therapy (Supplementary Table 6). When more than one sample per patient was available for antibiotic-versus-no-antibiotic comparison, the mean metabolite concentration was calculated.

IMM-RI

The IMM-RI was developed in analogy to the 'microbiome metabolite profile' in patients with COVID-19 (ref. 54). Five metabolites were selected according to univariate association with outcome (propionic acid, isovaleric acid, DAT and ICA) or biological plausibility (butyric acid). Metabolite levels at days +7–21 were used for the analysis. When more than one sample per patient was available, the mean metabolite concentration was used. Optimized thresholds for concentrations of individual metabolites were determined using the Youden index (Supplementary Table 9). If concentrations were beneath the cutoff, one point was assigned to that metabolite. A minimum of 0 points and a maximum of 5 points could be assigned to the IMM-RI. Patients were stratified into high and low IMM-RI groups according to their score (0–2, low IMM-RI; 3–5, high IMM-RI).

Analysis of clinical outcomes

MOFA factors. Patients were stratified according to peri-engraftment (days +7–21) factor values for factors 1, 3 and 4. Optimized thresholds were determined using the Youden index. The effect of factor values on OS was assessed via log-rank test, and hazard ratios were reported using the Cox regression model (Supplementary Table 3).

α-diversity. Patients were stratified into higher- and lower-diversity groups (above and below median diversity, respectively) according to the center-specific median inverse Simpson's diversity index during the peri-engraftment period. This practice is consistent with previous studies[7]. When more than one sample per patient was available, the mean inverse Simpson's diversity index was used. OS was analyzed using the Kaplan–Meier estimator. Cumulative incidences of relapse and TRM as well as GvHD and death were estimated, accounting for the competing risks of each of the respective endpoints (relapse versus TRM and GvHD versus death) in R based on the cmprsk package[67].

Immunomodulatory metabolite risk index. Patients were stratified into high and low IMM-RI groups. Cumulative incidence functions between groups were tested for equality using Gray's test[68], and the hazard ratio for the different endpoints was calculated in R based on the Fine-and-Gray model using the crr function[69] (TRM, GvHD) and the Cox regression model (OS) using SPSS 29.

Statistics and reproducibility

All patients receiving allo-SCT at MUC (between 2019 and 2021) and REG (between 2018 and 2021) were screened, and patients with a minimum of three longitudinal samples were included in the analysis. Samples obtained after day +100 after allo-SCT ($n = 2$) were excluded from the analysis, because the microbiome at these late time points is not comparable to that of the early post-transplantation period. No statistical method was used to predetermine sample sizes, but the size of our cohort ($n = 78$) is similar to those reported in previous publications[66]. Randomization did not apply in our non-interventional cohort. Data collection was not performed blind, and investigators were not blinded to outcome assessment. α-diversity metrics and metabolite levels were neither normally nor log-normally distributed as assessed by Shapiro–Wilk testing. Microsoft Excel and IBM

SPSS 29 were used for calculations and analyses. Further information on research design is available in the Nature Portfolio Reporting Summary linked to this article.

Bacteriome and fungome analysis

Extraction of nucleic acids. Stool (50 mg) was mixed with a pool of three spike bacteria, *Alcanivorax borkumensis*, *Agrobacterium radiobacter* and *Alicyclobacillus acidiphilus*, to 2×10^7, 1.6×10^7 and 6×10^8 16S ribosomal DNA (rDNA) copies per sample, respectively, which served as internal process controls[70]. Cells were lysed by applying a repeated bead-beating protocol using 0.5-mm yttria-stabilized zirconium oxide beads (MP Biomedicals) on a TissueLyser II instrument (Qiagen) followed by proteinase K digestion (Roche). DNA was purified by means of the MagNA Pure 96 instrument (Roche) using the MagNA Pure 96 DNA and Viral NA Large Volume Kit (Roche).

Amplification and sequencing of V1–V3 16S ribosomal DNA and fungal ITS1 regions. V1–V3 hypervariable regions of bacterial 16S rRNA genes were amplified from a total of 1×10^7 bacterial 16S rDNA copies for each sample using the forward primer S-D-Bact-0008-c-S-20 containing a sample-specific barcode and sequencing adaptor sequences together with the reverse primer S-D-Bact-0517-a-A-18 containing a 3′-P1 adaptor sequence. Fungal ITS1 regions were amplified from 5 ng DNA using the primer pair ITS1-30F and ITS1-217R[71] containing barcode and sequencing adaptors. The resulting amplicons were purified with MagSi-NGS^{PREP} Plus beads (Steinbrenner Laborsysteme). Amplicon copy numbers were determined using the KAPA Library Quantification Ion Torrent Kit (Roche). The DNA library was prepared by pooling adaptor-labeled amplicons at equimolar concentrations. Re-amplification of the final sequencing library by isothermal amplification, chip loading and high-throughput sequencing was carried out using the Ion Chef instrument and the Ion Torrent GeneStudio S5 Plus sequencer (Thermo Fisher Scientific).

Quantification. Bacterial and fungal DNA was quantified by real-time PCR using pan-bacterial (16S)- and pan-fungal (28S)-specific primers, respectively, and amplicon copy numbers were normalized to g of stool. Quantification of 16S rDNA copies by qPCR was carried out as published[72]. Fungal load was quantified by using primers NL-1 and 260R and a 28S rDNA-specific FAM-labeled hydrolysis probe[73]. DNA fragments of *Penicillium roqueforti* 28S rDNA amplified with NL-1 and NL-4 primers, which were cloned into the pJET1.2 vector (Thermo Fisher Scientific), were used as the quantification standard.

Data analysis. Raw sequencing reads were subjected to Trimmomatic[74] (0.39) for sliding window trimming, applying a window size of 25 and a quality cutoff of 20. Cutadapt[75] (3.4) was used for demultiplexing and removal of sequencing adaptors and 16S-specific PCR primer sequences. zOTUs were generated in R (4.2) from demultiplexed reads using a vsearch-based workflow[76]. Standard parameters were used, except for an expected error cutoff of 5 and an α value of 2. Taxonomy of zOTUs was predicted using the IDTAXA algorithm of the DECIPHER[77] package after matching to the All-Species Living Tree 16S reference database release 01_2022 (bacteria). The February 2020 release of the UNITE database[78] (fungal ITS1) was used to predict fungal taxonomy. α- and β-diversity analyses were conducted by applying the phyloseq[79] package v.1.36. Species richness was represented by summarized zOTUs. Means of groups were compared with the Wilcoxon rank-sum test (two sided) adjusted for multiple comparisons with the Benjamini–Hochberg procedure. β-diversity was calculated by weighted UniFrac, and distances between time points or groups (no antibiotic versus antibiotics, no GI-GvHD versus GI-GvHD) were projected in a principal-coordinate analysis (PCoA). Principal coordinates were calculated from weighted UniFrac distances after cumulative sum scaling of zOTU counts. The significance of group differences was analyzed by permutational multivariate analysis of variance (PERMANOVA) using the pairwiseAdonis[80] (0.4) package. Differential abundant features were identified with MaAsLin 2 release 1.7.3 (ref. 81) after total sum scaling and log transformation of zOTU counts. An α level of 0.05 was applied to *P* values, which were adjusted by the Benjamini–Hochberg method. Individual patients were applied as random effects for calculating the linear model. Plots were generated by ggpubr (0.4).

Whole shotgun metagenomic sequencing. DNA was extracted from stabilized stool samples as described above with the exception of adding bacterial spike controls to the sample. A total of 150 ng DNA was used and sheared to a mean length of 150 bp using the M220 Focused-ultrasonicator (Covaris), followed by size selection with MagSi-NGS^{PREP} Plus beads (Steinbrenner Laborsysteme) using 1.1× and 1.7× DNA-to-bead ratios. The Ion Plus Fragment Library Kit (Thermo Fisher Scientific) was used for end repair and ligation of sequencing adaptors. Sample-specific Ion Xpress barcodes were added to DNA fragments by ligation. Resulting libraries were quantified with the Ion Library TaqMan Quantitation Kit (Thermo Fisher Scientific). Samples were re-amplified with ten PCR cycles, followed by requantification as described above. Samples were mixed at equimolar ratios, and the resulting sequencing library pool was subjected to sequencing using the Ion Chef in combination with the Ion Torrent GeneStudio S5 Plus sequencer (Thermo Fisher Scientific) and the Ion 550 Chip Kit. Samples were sequenced to a mean sequencing depth of 6 million reads per samples. Raw sequencing counts were filtered for quality using Trimmomatic 0.39 with a read-length cutoff of 100 bp and a sliding window of 10 with a quality value of 15. Sequencing adaptors were removed with cutadapt 3.4. Human sequences were removed with Bowtie 2 by mapping to the GRCh38 (hg38) genome. MetaPhlAn 4 (ref. 82) and the ChocoPhlAn v.296 pangenome database were used to assign microbial taxonomy to sequences. The HMP Unified Metabolic Analysis Network 3 (HUMAnN3 (ref. 83)) was used to predict functional information by mapping to the UniRef90 database v.201901b. Predicted gene families were mapped to the MetaCyc[84] database for pathway-based analysis and the KEGG[85] database for gene family-level analysis, respectively (Supplementary Table 5). MaAsLin 2 (ref. 82) was used to identify significantly differential abundant metabolic (HUMAnN3) or taxonomic (MetaPhlAn 4) features from log-transformed relative abundances. The intestinal IMM-RI or MOFA factor levels 1 and 3 were used as fixed effects, and individual patients were used as random effects for the linear model, applying an α value of 0.25 for Benjamini–Hochberg procedure-corrected *P* values. Relative abundances were summed for MetaCyc superclasses for all pathways comprising them (Supplementary Table 5).

Virome analysis

Extraction of nucleic acids. Stool samples were mixed with 10 ml of filtered phage SM buffer, vortexed vigorously for 4 h at 4 °C and then centrifuged at 4,000*g* for 30 min to collect supernatant. The supernatant was passed through 0.22-µm filters (PES Membrane, ROCB29300, Merck Millipore) to remove bacterial-associated particles, and the volume was subsequently concentrated to less than 50 µl with Amicon Ultra Centrifugal Filters (10 kDa, R9EA18187, Merck Millipore). Next, 1/5 volume of chloroform was mixed with the samples, which were centrifuged at 14,000*g* for 3 min; the upper phase was retained, followed by DNase I (1 U μl^{-1}, 1158858, Invitrogen) treatment for 1 h at 37 °C to remove non-phage DNA. DNase I was inactivated by adding EDTA (0.1 M). Subsequently, lysis buffer (700 µl KOH stock (0.43 g per 10 ml), 430 µl DDT stock (0.8 g per 10 ml) and 370 µl water, pH 12) was added to the reaction, which was incubated at room temperature for 10 min followed by a 2-h incubation at −80 °C and for 5 min at 55 °C. Lysed VLPs were then treated for 30 min at 55 °C with proteinase K (20 mg ml^{-1}, 1112907, Invitrogen) to digest the remaining viral capsid and extract virome DNA. AMPure beads (Agencourt, Beckman Coulter)

were added to the extracted DNA, and samples were incubated for 15 min at room temperature. DNA was eluted from the beads with 35 µl Tris buffer (10 mM, pH 9.8) and stored at −80 °C. Sequencing was performed on an Illumina NovaSeq PE150 platform.

Virome sequence processing. Virome sequencing data were analyzed using the ViroProfiler pipeline[86]. Raw reads were processed with fastp (v.0.20.1) to remove adaptors and low-quality bases. The remaining reads were deduplicated using dedupe.sh from the BBMap suite (v.38.76) (https://sourceforge.net/projects/bbmap). The obtained reads were assembled into contigs using metaSPAdes (v.3.14.0)[87] with default parameters, retaining only contigs longer than 1 kb. Redundant contigs were removed using dedupe.sh. The remaining contigs were used to predict viral sequences with the combination of VirSorter2 (ref. 88), CAT (v.5.0.4)[89] and DeepVirFinder (v.1.0)[90]. Contigs predicted as category 1 and 2 by VirSorter2 or predicted as viruses by CAT were classified as viruses. Contigs were also classified as viruses if they were predicted as category 3 by VirSorter2 or could not be classified to taxonomy by CAT but were predicted as a virus by DeepVirFinder with q value < 0.01. To further reduce the redundancy of the contig library, we clustered contigs following the 'rapid genome clustering based on pairwise ANI' protocol in CheckV, which ensures that contigs in the same cluster share more than 95% identity and 80% coverage on short contigs. The longest contig of each cluster was selected as a representative for downstream analysis. Clean reads of each sample were mapped to the representative contigs using minimap2. Abundance profiles including read counts and TPM were calculated using CoverM (v.0.6.1) (https://github.com/wwood/CoverM). Viral bins were constructed using PHAMB[91]. The abundance of each bin was obtained by aggregate abundance of their contig members. Open reading frames were predicted using Prodigal (v.2.6.3) and provided to vConTACT2 (ref. 92) for taxonomy annotation. For contigs and bins that could not be assigned a taxonomy by vConTACT2, CAT annotations were used.

Data analysis. Viral richness (Ace) and diversity (inverse Simpson's diversity index) analyses and PCoA based on 'Bray–Curtis' similarities were conducted using the vegan package in R (v.4.0.2). The significant difference in PCoA was determined by PERMANOVA. Means of groups were compared with either Kruskal–Wallis with Dunn's post hoc test or the Wilcoxon rank-sum test (two sided) adjusted for multiple comparisons using the 'Bonferroni–Holm' method. The corr.test function in the Psych R package v.2.1.9 was used to compute Pearson correlation, and multiple comparisons were corrected using the Holm method ($\alpha = 0.05$). Graphs were generated in GraphPad Prism v.9 and the R ggplot2 package.

***BCoAT* phylogenetic analysis in the virome.** *BCoAT* was identified in viral genes using hmmscan searching against the HMM profile model of *BCoAT* in the NCBI protein family database (accession TIGR03948.1). There are two viral contigs that contain *BCoAT* genes, each of them in a VC cluster that contains more than one member contig (VC-1 belongs to viral cluster VC_804_0, and VC-2 belongs to VC_1122_0). Homologous genes of bacteriophage-coded *BCoAT* were obtained using MMseqs2 (ref. 93) to search against the NCBI NR database. Obtained homologous protein sequences were aligned using MAFFT v.7.475 and trimmed with trimAl v.1.4.rev15 to remove bases with <50% coverage, and a phylogenetic tree was created using FastTree v.2.1.10 (ref. 94). The phylogenetic tree was visualized using the ggtree package in R.

Viral gene annotation and genome comparison. Viral genomes of VC-1 and VC-2 were annotated using the PHROGs database[95] and visualized with pyCircos (https://github.com/ponnhide/pyCircos). The closest related bacterial gene to VC-1 and VC-2 on the *BCoAT* phylogenetic tree was selected as the reference genome. tBLASTx was used to compare it to the viral contig. The gggenomes package in R (https://github.com/thackl/gggenomes) was used to visualize the results of the comparison, with lines representing the protein sequence identity determined by tBLASTx.

Metabolome analysis

Sample preparation for targeted analysis. Approximately 100 mg of stool was weighed in a 15-ml bead-beater tube (CKMix50, 15 ml, Bertin Technologies) filled with 2.8-mm and 5.0-mm ceramic beads (i.d.). Methanol-based dehydrocholic acid extraction solvent (5 ml, $c = 1.3$ µmol l^{-1}) was added as an internal standard for work-up losses. Samples were extracted with a bead beater (Precellys Evolution, Bertin Technologies) supplied with a Cryolys cooling module three times each for 20 s with 15-s breaks in between at 10,000 r.p.m. The fecal suspension (1 ml) was dried in a vacuum centrifuge (Eppendorf Vacufuge) to determine the dry weight.

Measurement of SCFAs, lactic acid, desaminotyrosine and indole-3-carboxyaldehyde (panel 1). The 3-NPH method was used for quantitation of SCFAs as well as lactic acid, DAT and indole-3-carboxyaldehyde[96]. Briefly, 40 µl of the fecal extract and 15 µl of 50 µM isotopically labeled standards were mixed with 20 µl of 120 mM EDC HCl–6% pyridine solution and 20 µl of 200 mM 3-NPH HCl solution. After 30 min at 40 °C with shaking at 1,000 r.p.m. using an Eppendorf ThermoMixer (Eppendorf), 900 µl acetonitrile–water (50/50, vol/vol) was added. After centrifugation at 13,000 revolutions per minute U min^{-1} for 2 min, the clear supernatant was used for analysis. The measurement was performed using a QTRAP 5500 triple quadrupole mass spectrometer (SCIEX) coupled to an ExionLC AD (SCIEX) ultrahigh-performance liquid chromatography system. The electrospray voltage was −4,500 V, curtain gas was at 35 psi, ion source gas 1 was at 55 psi, ion source gas 2 was at 65 psi, and the temperature was 500 °C. Multiple-reaction-monitoring parameters were optimized using commercially available standards. Chromatographic separation was performed on a 1.7-µm, 100 × 2.1-mm, 100 Å Kinetex C18 column (Phenomenex) with 0.1% formic acid (eluent A) and 0.1% formic acid in acetonitrile (eluent B) as elution solvents. An injection volume of 1 µl and a flow rate of 0.4 ml min^{-1} were used. The gradient elution started at 23% B, which was held for 3 min; afterward the concentration was increased to 30% B at 4 min, with another increase to 40% B at 6.5 min; at 7 min, 100% B was used, which was held for 1 min; at 8.5 min, the column was equilibrated at starting conditions. The column oven was set to 40 °C, and the autosampler was set to 15 °C. Data acquisition and instrumental control were performed with Analyst 1.7 software (SCIEX). Data were analyzed with MultiQuant 3.0.3 (SCIEX) and MetaboAnalyst[97]. Features with more than 70% of missing values were removed. Missing values were replaced by LoDs (1/5 of the minimum positive value of each variable). Heatmaps were generated after normalization by log transformation (base 10). Means of multiple groups (time points) were compared with the Kruskal–Wallis test followed by Dunn's multiple-comparison test. Comparisons between two groups (no antibiotic versus antibiotics, no GI-GvHD versus GI-GvHD) were performed with the Wilcoxon matched-pair signed-rank test or the Mann–Whitney test, respectively (two sided, 95% confidence level). Graphs and statistics were created in Prism 9 (GraphPad).

Measurement of bile acids (panel 2). BA analysis was performed according to Reiter et al.[98]. Briefly, 20 µl of isotopically labeled BAs (approximately 7 µM each) were added to 100 µl of fecal extract. Targeted BA measurement was performed using the same system as described above. A multiple-reaction-monitoring method was used for detection and quantification of BAs[98]. An electrospray ion voltage of −4,500 V and the following ion source parameters were used: curtain gas (35 psi), temperature (450 °C), gas 1 (55 psi), gas 2 (65 psi) and

entrance potential (−10 V). MS parameters and LC conditions were optimized using commercially available standards of endogenous BAs and deuterated BAs for simultaneous quantification of the selected 34 analytes. For separation of analytes, a 100 × 2.1-mm, 100 Å, 1.7-µm, Kinetex C18 column (Phenomenex) was used. Chromatographic separation was performed with a constant flow rate of 0.4 ml min^{-1} using a mobile phase consisting of water (eluent A) and acetonitrile–water (95/5, vol/vol, eluent B), both containing 5 mM ammonium acetate and 0.1% formic acid. The gradient elution started with 25% B for 2 min, increased at 3.5 min to 27% B and in 2 min to 35% B, which was held until 10 min, increased in 1 min to 43% B, held for 1 min, increased in 2 min to 58% B and held 3 min isocratically at 58% B, and then the concentration was increased to 65% at 17.5 min, with another increase to 80% B at 18 min, followed by an increase at 19 min to 100% B, which was held for 1 min; at 20.5 min, the column was equilibrated for 4.5 min at starting conditions. The injection volume for all samples was 1 µl, the column oven temperature was set to 40 °C, and the autosampler was kept at 15 °C. Data acquisition and instrumental control were performed with Analyst 1.7 software (SCIEX). Data were analyzed as indicated for panel 1.

Multiomic factor analysis. Details on MOFA methodology and downstream analysis can be found in Supplementary Note 1 and the original publication[99].

As input for the MOFA model, we used bacterial 16S rRNA (239 features), fungal ITS1 rRNA (154 features) ASVs and assembled viral clusters (434 features) as well as metabolite concentrations from targeted metabolomics (28 features; metabolites with missing values in more than 90% of samples were excluded from the model). Please refer to Supplementary Note 1 for a description of the pipeline used to generate ASVs for MOFA. All inputs were normalized by centralized log normalization (microbiome and virome data) or log transformation (base 10, metabolomics data). When fitting the model, we selected for the top factors ordered by the mean fractional variance explained across omic modalities (that is, factor 1 contributed the most, and factor 10 contributed the least to mean fractional variation; Fig. 3b).

When testing factor values for statistically significant differences between groups (clinical metadata, IMM-RI and *BCoAT* data), a two-tailed Mann–Whitney *U*-test was used. The mean of factor values of days +7–21 after allo-SCT of a given patient were used for testing. In cases in which different group assignment was possible for the same patient for different time points (for example, *BCoAT* gene copies detected at day 7 but not at day 14), the patient was assigned to the group showing the characteristic, if the characteristic was detected for at least one time point. The resulting *P* values were corrected for multiple testing using the FDR approach[100] across all hypotheses for which factor values were analyzed for association with clinical metadata, IMM-RI or *BCoAT* data.

To assess time-dependent variations, we fitted a MEFISTO[25] model on the MOFA input data, with time points in days relative to allo-SCT as the covariate. Due to sparseness, time points after day 35 were combined to a single time point.

MOFA–MEFISTO was performed using R (4.1.1) and Python (3.6.13). The MOFA–MEFISTO model was trained using the MOFA2 R package (1.4.0)[99] as an interface to the mofapy2 Python package (0.6.4). Scale differences between views were not pronounced; therefore MOFA input modalities were not scaled to unit variance. The number of factors was set to 10, and convergence was set to medium. Downstream analysis of MOFA, statistical testing and plotting were performed in R, using the packages MOFA2 (1.4.0), ggplot2 (3.3.5), ggpubr (0.4.0), corrplot (0.91) and rstatix (0.7.0).

Reporting summary

Further information on research design is available in the Nature Portfolio Reporting Summary linked to this article.

Data availability

Microbial sequencing (bacterial and fungal amplicon data and viral metagenomic sequencing data) that support the findings of this study have been deposited at the European Nucleotide Archive under accession number PRJEB53547 (https://www.ebi.ac.uk/ena/browser/view/PRJEB53547). MS data have been deposited at Zenodo under accession number 6603017 (https://zenodo.org/record/6603017). Both repositories are annotated with clinical metadata. All other data supporting the findings of this study are available from the corresponding author on reasonable request. The stool samples analyzed in this study comprised a unique biosample collection and have been expended for the analyses performed in this study. No additional material is available. Source data are provided with this paper.

Code availability

The scripts and packages used for whole shotgun metagenomic sequencing, viral metagenomic sequencing and MOFA have been deposited at GitHub (https://github.com/guardianre/MOFA-in-allo-SCT.git).

References

1. Zeiser, R. & Blazar, B. R. Acute graft-versus-host disease — biologic process, prevention, and therapy. *N. Engl. J. Med.* **377**, 2167–2179 (2017).
2. Holler, E. et al. Metagenomic analysis of the stool microbiome in patients receiving allogeneic stem cell transplantation: loss of diversity is associated with use of systemic antibiotics and more pronounced in gastrointestinal graft-versus-host disease. *Biol. Blood Marrow Transpl.* **20**, 640–645 (2014).
3. Stoma, I. et al. Compositional flux within the intestinal microbiota and risk for bloodstream infection with gram-negative bacteria. *Clin. Infect. Dis.* **73**, e4627–e4635 (2021).
4. Golob, J. L. et al. Stool microbiota at neutrophil recovery is predictive for severe acute graft vs host disease after hematopoietic cell transplantation. *Clin. Infect. Dis.* **65**, 1984–1991 (2017).
5. Malard, F., Gasc, C., Plantamura, E. & Doré, J. High gastrointestinal microbial diversity and clinical outcome in graft-versus-host disease patients. *Bone Marrow Transplant.* **53**, 1493–1497 (2018).
6. Weber, D. et al. Microbiota disruption induced by early use of broad-spectrum antibiotics is an independent risk factor of outcome after allogeneic stem cell transplantation. *Biol. Blood Marrow Transplant.* **23**, 845–852 (2017).
7. Peled, J. U. et al. Microbiota as predictor of mortality in allogeneic hematopoietic-cell transplantation. *N. Engl. J. Med.* **382**, 822–834 (2020).
8. Shono, Y. et al. Increased GVHD-related mortality with broad-spectrum antibiotic use after allogeneic hematopoietic stem cell transplantation in human patients and mice. *Sci. Transl. Med.* **8**, 339ra71 (2016).
9. Stein-Thoeringer, C. K. et al. Lactose drives *Enterococcus* expansion to promote graft-versus-host disease. *Science* **366**, 1143–1149 (2019).
10. Jenq, R. R. et al. Regulation of intestinal inflammation by microbiota following allogeneic bone marrow transplantation. *J. Exp. Med.* **209**, 903–911 (2012).
11. Mathewson, N. D. et al. Gut microbiome-derived metabolites modulate intestinal epithelial cell damage and mitigate graft-versus-host disease. *Nat. Immunol.* **17**, 505–513 (2016).
12. Swimm, A. et al. Indoles derived from intestinal microbiota act via type I interferon signaling to limit graft-versus-host disease. *Blood* **132**, 2506–2519 (2018).
13. Campbell, C. et al. Bacterial metabolism of bile acids promotes generation of peripheral regulatory T cells. *Nature* **581**, 475–479 (2020).
14. Payen, M. et al. Functional and phylogenetic alterations in gut microbiome are linked to graft-versus-host disease severity. *Blood Adv.* **4**, 1824–1832 (2020).

15. Michonneau, D. et al. Metabolomics analysis of human acute graft-versus-host disease reveals changes in host and microbiota-derived metabolites. *Nat. Commun.* **10**, 5695 (2019).
16. Markey, K. A. et al. The microbe-derived short-chain fatty acids butyrate and propionate are associated with protection from chronic GVHD. *Blood* **136**, 130–136 (2020).
17. Peters, S. G., Pomare, E. W. & Fisher, C. A. Portal and peripheral blood short chain fatty acid concentrations after caecal lactulose instillation at surgery. *Gut* **33**, 1249–1252 (1992).
18. Boets, E. et al. Systemic availability and metabolism of colonic-derived short-chain fatty acids in healthy subjects: a stable isotope study: short-chain fatty acid systemic availability and metabolism in humans. *J. Physiol.* **595**, 541–555 (2017).
19. Wang, R. X., Lee, J. S., Campbell, E. L. & Colgan, S. P. Microbiota-derived butyrate dynamically regulates intestinal homeostasis through regulation of actin-associated protein synaptopodin. *Proc. Natl Acad. Sci. USA* **117**, 11648–11657 (2020).
20. Kieft, K. et al. Ecology of inorganic sulfur auxiliary metabolism in widespread bacteriophages. *Nat. Commun.* **12**, 3503 (2021).
21. Chen, L. X. et al. Large freshwater phages with the potential to augment aerobic methane oxidation. *Nat. Microbiol.* **5**, 1504–1515 (2020).
22. Howard-Varona, C. et al. Phage-specific metabolic reprogramming of virocells. *ISME J.* **14**, 881–895 (2020).
23. Zanella, M. C. et al. Unmasking viral sequences by metagenomic next-generation sequencing in adult human blood samples during steroid-refractory/dependent graft-versus-host disease. *Microbiome* **9**, 28 (2021).
24. Legoff, J. et al. The eukaryotic gut virome in hematopoietic stem cell transplantation: new clues in enteric graft-versus-host disease. *Nat. Med.* **23**, 1080–1085 (2017).
25. Velten, B. et al. Identifying temporal and spatial patterns of variation from multimodal data using MEFISTO. *Nat. Methods* **19**, 179–186 (2022).
26. Ruutu, T. et al. Improved survival with ursodeoxycholic acid prophylaxis in allogeneic stem cell transplantation: long-term follow-up of a randomized study. *Biol. Blood Marrow Transplant.* **20**, 135–138 (2014).
27. Haring, E. et al. Bile acids regulate intestinal antigen presentation and reduce graft-versus-host disease without impairing the graft-versus-leukemia effect. *Haematologica* **106**, 2131–2146 (2021).
28. Alwin, A. & Karst, S. M. The influence of microbiota-derived metabolites on viral infections. *Curr. Opin. Virol.* **49**, 151–156 (2021).
29. Liu, L. et al. Improved production of propionic acid in *Propionibacterium jensenii* via combinational overexpression of glycerol dehydrogenase and malate dehydrogenase from *Klebsiella pneumoniae*. *Appl. Environ. Microbiol.* **81**, 2256–2264 (2015).
30. Molinaro, A. et al. Imidazole propionate is increased in diabetes and associated with dietary patterns and altered microbial ecology. *Nat. Commun.* **11**, 5881 (2020).
31. Mager, L. F. et al. Microbiome-derived inosine modulates response to checkpoint inhibitor immunotherapy. *Science* **369**, 1481–1489 (2020).
32. Dubin, K. et al. Intestinal microbiome analyses identify melanoma patients at risk for checkpoint-blockade-induced colitis. *Nat. Commun.* **7**, 10391 (2016).
33. Pryde, S. E., Duncan, S. H., Hold, G. L., Stewart, C. S. & Flint, H. J. The microbiology of butyrate formation in the human colon. *FEMS Microbiol. Lett.* **217**, 133–139 (2002).
34. Meedt, E. et al. Prolonged suppression of butyrate producing bacteria is associated with acute gastrointestinal graft-versus-host disease and transplant related mortality after allogeneic stem cell transplantation. *Clin. Infect. Dis.* **74**, 614–621 (2022).
35. Tisza, M. J. & Buck, C. B. A catalog of tens of thousands of viruses from human metagenomes reveals hidden associations with chronic diseases. *Proc. Natl Acad. Sci. USA* **118**, e2023202118 (2021).
36. Redder, P., Hausmann, S., Khemici, V., Yasrebi, H. & Linder, P. Bacterial versatility requires DEAD-box RNA helicases. *FEMS Microbiol. Rev.* **39**, 392–412 (2015).
37. Hatfull, G. F. & Hendrix, R. W. Bacteriophages and their genomes. *Curr. Opin. Virol.* **1**, 298–303 (2011).
38. Weber, D. et al. Reg3α levels at day of allogeneic stem cell transplantation predict outcome and correlate with early antibiotic use. *Blood Adv.* **7**, 1326–1335 (2023).
39. Seike, K. et al. Ambient oxygen levels regulate intestinal dysbiosis and GVHD severity after allogeneic stem cell transplantation. *Immunity* **56**, 353–368 (2023).
40. Tamanai-Shacoori, Z. et al. *Roseburia* spp.: a marker of health? *Future Microbiol.* **12**, 157–170 (2017).
41. Ogita, T. et al. Oral administration of *Flavonifractor plautii* strongly suppresses T_H2 immune responses in mice. *Front. Immunol.* **11**, 379 (2020).
42. Stephen, A. M. & Cummings, J. H. The microbial contribution to human faecal mass. *J. Med. Microbiol.* **13**, 45–56 (1980).
43. Haak, B. W. et al. Integrative transkingdom analysis of the gut microbiome in antibiotic perturbation and critical illness. *mSystems* **6**, e01148-20 (2021).
44. Rolling, T. et al. Haematopoietic cell transplantation outcomes are linked to intestinal mycobiota dynamics and an expansion of *Candida parapsilosis* complex species. *Nat. Microbiol.* **6**, 1505–1515 (2021).
45. van der Velden, W. J. F. M. et al. Role of the mycobiome in human acute graft-versus-host disease. *Biol. Blood Marrow Transplant.* **19**, 329–332 (2013).
46. Fujiwara, H. et al. Microbial metabolite sensor GPR43 controls severity of experimental GVHD. *Nat. Commun.* **9**, 3674 (2018).
47. Dubouchet, L. et al. Operational tolerance after hematopoietic stem cell transplantation is characterized by distinct transcriptional, phenotypic, and metabolic signatures. *Sci. Transl. Med.* **14**, eabg3083 (2022).
48. Steed, A. L. et al. The microbial metabolite desaminotyrosine protects from influenza through type I interferon. *Science* **357**, 498–502 (2017).
49. Pols, T. W. H. et al. Lithocholic acid controls adaptive immune responses by inhibition of T_H1 activation through the vitamin D receptor. *PLoS ONE* **12**, e0176715 (2017).
50. Winkler, E. S. et al. The intestinal microbiome restricts alphavirus infection and dissemination through a bile acid-type I IFN signaling axis. *Cell* **182**, 901–918 (2020).
51. Fischer, J. C. et al. Type I interferon signaling before hematopoietic stem cell transplantation lowers donor T cell activation via reduced allogenicity of recipient cells. *Sci. Rep.* **9**, 14955 (2019).
52. Puccetti, M. et al. Enteric formulated indole-3-carboxaldehyde targets the aryl hydrocarbon receptor for protection in a murine model of metabolic syndrome. *Int. J. Pharm.* **602**, 120610 (2021).
53. Li, W. et al. A bacterial bile acid metabolite modulates T_{reg} activity through the nuclear hormone receptor NR4A1. *Cell Host Microbe* **29**, 1366–1377 (2021).
54. Stutz, M. R. et al. Immunomodulatory fecal metabolites are associated with mortality in COVID-19 patients with respiratory failure. *Nat. Commun.* **13**, 6615 (2022).
55. Lee, J. et al. Gut microbiota-derived short-chain fatty acids promote poststroke recovery in aged mice. *Circ. Res.* **127**, 453–465 (2020).
56. Norona, J. et al. Glucagon-like peptide 2 for intestinal stem cell and Paneth cell repair during graft-versus-host disease in mice and humans. *Blood* **136**, 1442–1455 (2020).

57. Henden, A. S. et al. Pegylated interferon-2α invokes graft-versus-leukemia effects in patients relapsing after allogeneic stem cell transplantation. *Blood Adv.* **3**, 3013–3019 (2019).
58. Peled, J. U. et al. Intestinal microbiota and relapse after hematopoietic-cell transplantation. *J. Clin. Oncol.* **35**, 1650–1659 (2017).
59. Thevaranjan, N. et al. Age-associated microbial dysbiosis promotes intestinal permeability, systemic inflammation, and macrophage dysfunction. *Cell Host Microbe* **21**, 455–466 (2017).
60. Vital, M., Howe, A. C. & Tiedje, J. M. Revealing the bacterial butyrate synthesis pathways by analyzing (meta)genomic data. *mBio* **5**, e00889 (2014).
61. Weinbauer, M. & Suttle, C. Lysogeny and prophage induction in coastal and offshore bacterial communities. *Aquat. Microb. Ecol.* **18**, 217–225 (1999).
62. Romick-Rosendale, L. E. et al. Antibiotic exposure and reduced short chain fatty acid production after hematopoietic stem cell transplant. *Biol. Blood Marrow Transplant.* **24**, 2418–2424 (2018).
63. Smith, M. et al. Gut microbiome correlates of response and toxicity following anti-CD19 CAR T cell therapy. *Nat. Med.* **28**, 713–723 (2022).
64. Routy, B. et al. Gut microbiome influences efficacy of PD-1-based immunotherapy against epithelial tumors. *Science* **359**, 91–97 (2018).
65. Ma, T. et al. Differences in gut virome related to Barrett esophagus and esophageal adenocarcinoma. *Microorganisms* **9**, 1701 (2021).
66. Taur, Y. et al. The effects of intestinal tract bacterial diversity on mortality following allogeneic hematopoietic stem cell transplantation. *Blood* **124**, 1174–1182 (2014).
67. Scrucca, L., Santucci, A. & Aversa, F. Competing risk analysis using R: an easy guide for clinicians. *Bone Marrow Transplant.* **40**, 381–387 (2007).
68. Gray, R. J. A class of *K*-sample tests for comparing the cumulative incidence of a competing risk. *Ann. Stat.* **16**, 1141–1154 (1988).
69. Scrucca, L., Santucci, A. & Aversa, F. Regression modeling of competing risk using R: an in depth guide for clinicians. *Bone Marrow Transplant.* **45**, 1388–1395 (2010).
70. Stämmler, F. et al. Adjusting microbiome profiles for differences in microbial load by spike-in bacteria. *Microbiome* **4**, 28 (2016).
71. Usyk, M., Zolnik, C. P., Patel, H., Levi, M. H. & Burk, R. D. Novel ITS1 fungal primers for characterization of the mycobiome. *mSphere* **2**, e00488-17 (2017).
72. Wahida, A. et al. XIAP restrains TNF-driven intestinal inflammation and dysbiosis by promoting innate immune responses of Paneth and dendritic cells. *Sci. Immunol.* **6**, eabf7235 (2021).
73. Vollmer, T., Störmer, M., Kleesiek, K. & Dreier, J. Evaluation of novel broad-range real-time PCR assay for rapid detection of human pathogenic fungi in various clinical specimens. *J. Clin. Microbiol.* **46**, 1919–1926 (2008).
74. Bolger, A. M., Lohse, M. & Usadel, B. Trimmomatic: a flexible trimmer for Illumina sequence data. *Bioinformatics* **30**, 2114–2120 (2014).
75. Martin, M. Cutadapt removes adapter sequences from high-throughput sequencing reads. *EMBnet J.* **17**, 10 (2011).
76. Callahan, B. J., Sankaran, K., Fukuyama, J. A., McMurdie, P. J. & Holmes, S. P. Bioconductor workflow for microbiome data analysis: from raw reads to community analyses. *F1000Res.* **5**, 1492 (2016).
77. Murali, A., Bhargava, A. & Wright, E. S. IDTAXA: a novel approach for accurate taxonomic classification of microbiome sequences. *Microbiome* **6**, 140 (2018).
78. Nilsson, R. H. et al. The UNITE database for molecular identification of fungi: handling dark taxa and parallel taxonomic classifications. *Nucleic Acids Res.* **47**, D259–D264 (2019).
79. McMurdie, P. J. & Holmes, S. phyloseq: an R package for reproducible interactive analysis and graphics of microbiome census data. *PLoS ONE* **8**, e61217 (2013).
80. Martinez, A. P. pairwiseAdonis: pairwise multilevel comparison using adonis. R package version 0.4 (2020).
81. Yarza, P. et al. The All-Species Living Tree project: a 16S rRNA-based phylogenetic tree of all sequenced type strains. *Syst. Appl. Microbiol.* **31**, 241–250 (2008).
82. Mallick, H. et al. Multivariable association discovery in population-scale meta-omics studies. *PLoS Comput. Biol.* **17**, e1009442 (2021).
83. Blanco-Miguez, A. et al. Extending and improving metagenomic taxonomic profiling with uncharacterized species with MetaPhlAn 4. *Nat. Biotechnol.* **41**, 1633–1644 (2023); https://doi.org/10.1038/s41587-023-01688-w
84. Beghini, F. et al. Integrating taxonomic, functional, and strain-level profiling of diverse microbial communities with bioBakery 3. *eLife* **10**, e65088 (2021).
85. Kanehisa, M. KEGG: Kyoto Encyclopedia of Genes and Genomes. *Nucleic Acids Res.* **28**, 27–30 (2000).
86. Ru, J., Khan Mirzaei, M., Xue, J., Peng, X. & Deng, L. ViroProfiler: a containerized bioinformatics pipeline for viral metagenomic data analysis. *Gut Microbes* **15**, 2192522 (2023).
87. Nurk, S., Meleshko, D., Korobeynikov, A. & Pevzner, P. A. metaSPAdes: a new versatile metagenomic assembler. *Genome Res.* **27**, 824–834 (2017).
88. Guo, J. et al. VirSorter2: a multi-classifier, expert-guided approach to detect diverse DNA and RNA viruses. *Microbiome* **9**, 37 (2021).
89. von Meijenfeldt, F. A. B., Arkhipova, K., Cambuy, D. D., Coutinho, F. H. & Dutilh, B. E. Robust taxonomic classification of uncharted microbial sequences and bins with CAT and BAT. *Genome Biol.* **20**, 217 (2019).
90. Ren, J. et al. Identifying viruses from metagenomic data using deep learning. *Quant. Biol.* **8**, 64–77 (2020).
91. Johansen, J. et al. Genome binning of viral entities from bulk metagenomics data. *Nat. Commun.* **13**, 965 (2022).
92. Bin Jang, H. et al. Taxonomic assignment of uncultivated prokaryotic virus genomes is enabled by gene-sharing networks. *Nat. Biotechnol.* **37**, 632–639 (2019).
93. Steinegger, M. & Söding, J. MMseqs2 enables sensitive protein sequence searching for the analysis of massive data sets. *Nat. Biotechnol.* **35**, 1026–1028 (2017).
94. Price, M. N., Dehal, P. S. & Arkin, A. P. FastTree 2 — approximately maximum-likelihood trees for large alignments. *PLoS ONE* **5**, e9490 (2010).
95. Terzian, P. et al. PHROG: families of prokaryotic virus proteins clustered using remote homology. *NAR Genom. Bioinform.* **3**, lqab067 (2021).
96. Weiss, A. S. et al. In vitro interaction network of a synthetic gut bacterial community. *ISME J.* **16**, 1095–1109 (2022).
97. Pang, Z. et al. MetaboAnalyst 5.0: narrowing the gap between raw spectra and functional insights. *Nucleic Acids Res.* **49**, W388–W396 (2021).
98. Reiter, S. et al. Development of a highly sensitive ultra-high-performance liquid chromatography coupled to electrospray ionization tandem mass spectrometry quantitation method for fecal bile acids and application on Crohn's disease studies. *J. Agric. Food Chem.* **69**, 5238–5251 (2021).
99. Argelaguet, R. et al. Multi-Omics Factor Analysis—a framework for unsupervised integration of multi-omics data sets. *Mol. Syst. Biol.* **14**, e8124 (2018).
100. Benjamini, Y. & Hochberg, Y. Controlling the false discovery rate: a practical and powerful approach to multiple testing. *J. R. Stat. Soc. B Methodol.* **57**, 289–300 (1995).

Acknowledgements

This study was supported by the Deutsche Forschungsgemeinschaft (Projektnummer 360372040—SFB 1335 (to S.H., H.P., K.S. and F.B.),

Projektnummer 395357507—SFB 1371 (to L.D., H.P., J. Ruland, E.T.O., J.C.F., K.-P.J., M.Q., K.S., S.J., D.H.B. and E.H.), Projektnummer 324392634—TRR 221 (to H.P., W.H., D.Wolff, M.E., D.Weber, A.G. and E.H.), Projektnummer 464797012—SPP 2330 (to L.D.), DE 2360/6-1 (to L.D.), BA 2851/6-1 (to F.B.), DE 2360/1-1 (Emmy Noether Program, to L.D.)), German Cancer Aid (70114547 to H.P.), the Wilhelm Sander Foundation (2021.040.1 to H.P.), the Bavarian Cancer Research Center (BZKF to H.P. and F.B.), the European Hematology Association (to H.P.), the Else Kröner-Fresenius-Stiftung (funding line, Else-Kröner Forschungskolleg to E.T.O. and E.M.), the Bavarian State Ministry of Science and Art (to H.P.), the DKMS Foundation for Giving Life (to H.P.), the German José Carreras Leukemia Foundation (grant DJCLS 01 GvHD/2016 to E.H.), the European Research Commission (project BCM-UPS, grant no. 682473 to F.B. and EU ERC StG—GA no. 803077 to L.D.), the Deutsches Konsortium für Translationale Krebsforschung (fellowship to E.T.O.) and the Deutsche Gesellschaft für Innere Medizin (fellowship to E.T.O.). H.P. is supported by the EMBO Young Investigator Program. We thank the REG allo-SCT team, especially H. Bremm, M. Caioni, T. Schifferstein and Y. Schumann for their help in collecting and cryopreserving stool samples and S. Gleich for data management. We express gratitude to the MUC allo-SCT team, especially K. Braitsch, K. Koch, L. Oßwald, K. Nickel and the entire D2a nursing staff for their excellency in sample acquisition. We acknowledge A. Conrad and W. Johannes (K.-P.J. laboratory) for help with biobanking and A. Wahida for logistical support as well as the MUC ColoBAC team: R. Schmid, M. Middelhoff, J. Horstmann and L. Fricke. We thank the tissue bank of MRI and TUM (MTBIO) for excellent technical support. We acknowledge R.R. Jenq for critical review of the manuscript.

Author contributions

Conceptualization: E.T.O., L.D., E.H., H.P. Methodology: J.Ru, A.H., J.X., M.G., K.K., S.J., D.H.B., K.S., M.Q. Formal analysis: E.T.O., E.M., A.H., J.X., P.Heinrich. Investigation: E.T.O., E.M., S. Ghimire, T.E., S. Göldel, A.S. Resources: C.S., D.Weber, D.Wolff, M.E., D.H.B., W.H., P.Herhaus, M.V., F.B., M.Q., K.-P.J. Data curation: E.T.O., E.M., M.T. Writing (original draft): E.T.O., E.M. Writing (review and editing): E.T.O., E.M., P.Heinrich, O.M., J.X., F.B., S. Göttert, S.L., J.C.F., S.H., M.R.M.v.d.B., L.D., E.H., H.P. Visualization: E.T.O., E.M., A.H., J.X., J.R., T.E., S. Göldel, A.S., P.Heinrich. Supervision: E.T.O., D.H.B., A.G., L.D., E.H. and H.P. Project administration: E.T.O., E.M. Contributions are specified according to CRediT (Contributor Roles Taxonomy). All authors read, revised and approved the final draft.

Competing interests

E.T.O.: honoraria (BeiGene), travel (BeiGene). M.R.M.v.d.B.: research support and stock options from Seres Therapeutics and stock options from Notch Therapeutics and Pluto Therapeutics; he has received royalties from Wolters Kluwer; he has consulted, received honorarium from or participated in advisory boards for Seres Therapeutics, Vor Biopharma, Rheos Medicines, Frazier Healthcare Partners, Nektar Therapeutics, Notch Therapeutics, Ceramedix, LyGenesis, Pluto Therapeutics, GlaxoSmithKline, Da Volterra, Thymofox, Garuda, Novartis (spouse), Synthekine (spouse), BeiGene (spouse), Kite (spouse); he has IP licensing with Seres Therapeutics and Juno Therapeutics; and he holds a fiduciary role on the foundation board of DKMS (a nonprofit organization). E.H.: scientific advisory board (MaaT Pharma, PharmaBiome (Novartis–Medac)), honoraria and research funding (Neovii, Novartis and Medac). H.P.: honoraria (Novartis, Gilead–Kite, AbbVie, Pfizer, MSD, Bristol Myers Squibb (BMS), Servier, Janssen-Cilag), travel (Janssen-Cilag, Novartis, AbbVie, Novartis, Jazz, Gilead–Kite, AMGEN), research (BMS). C.S.: honoraria (Lilly, Tillotts, Juvisé), research (Luvos). S.H. has been a consultant for BMS, Novartis, Merck, AbbVie and Roche; has received research funding from BMS and Novartis; and is an employee of and holds equity interest in Roche–Genentech. M.V.: honoraria from Novartis, Medac, AbbVie and Jazz Pharmaceuticals as well as travel grants from Medac, Gilead and Jazz Pharmaceuticals. A.S.: honoraria (BeiGene), travel (BeiGene). W.H.: honoraria (Amgen, Novartis), travel (Amgen, Janssen-Cilag). The remaining authors declare no competing interests.

Additional information

Extended data is available for this paper at https://doi.org/10.1038/s43018-023-00669-x.

Supplementary information The online version contains supplementary material available at https://doi.org/10.1038/s43018-023-00669-x.

Correspondence and requests for materials should be addressed to Erik Thiele Orberg or Hendrik Poeck.

Peer review information *Nature Cancer* thanks Stewart J. Anderson and Gerard Socie for their contribution to the peer review of this work.

Reprints and permissions information is available at www.nature.com/reprints.

Publisher's note Springer Nature remains neutral with regard to jurisdictional claims in published maps and institutional affiliations.

Erik Thiele Orberg[1,2,3,25] ✉, Elisabeth Meedt[4,25], Andreas Hiergeist[5,25], Jinling Xue[6,7,25], Paul Heinrich[4,8], Jinlong Ru[6,7], Sakhila Ghimire[4], Oriana Miltiadous[9], Sarah Lindner[10], Melanie Tiefgraber[1], Sophia Göldel[1], Tina Eismann[1], Alix Schwarz[1], Sascha Göttert[4], Sebastian Jarosch[11], Katja Steiger[2,12,13], Christian Schulz[14,15], Michael Gigl[16], Julius C. Fischer[17], Klaus-Peter Janssen[18], Michael Quante[19], Simon Heidegger[1,3], Peter Herhaus[1], Mareike Verbeek[1], Jürgen Ruland[2,3,20], Marcel R. M. van den Brink[10,21,22], Daniela Weber[4], Matthias Edinger[4,8], Daniel Wolff[4], Dirk H. Busch[11,15], Karin Kleigrewe[16], Wolfgang Herr[4], Florian Bassermann[1,2,3,23], André Gessner[5,25], Li Deng[6,7,25], Ernst Holler[4,25] & Hendrik Poeck[4,8,24,25] ✉

[1]Department of Internal Medicine III, School of Medicine, Technical University of Munich, Klinikum rechts der Isar, Munich, Germany. [2]German Cancer Consortium (DKTK), partner-site Munich, a partnership between DKFZ and Klinikum rechts der Isar, Munich, Germany. [3]Center for Translational Cancer Research (TranslaTUM), School of Medicine, Technical University of Munich, Munich, Germany. [4]Department of Internal Medicine III, Hematology and Medical Oncology, University Medical Center, Regensburg, Germany. [5]Institute of Clinical Microbiology and Hygiene, University Medical Center, Regensburg, Germany. [6]Institute of Virology, Helmholtz Zentrum Munich, Munich, Germany. [7]Chair of Prevention for Microbial Infectious Disease, Central

Institute of Disease Prevention and School of Life Sciences, Technical University of Munich, Munich, Germany. [8]Leibniz Institute for Immunotherapy, Regensburg, Germany. [9]Department of Pediatrics, Memorial Sloan Kettering Cancer Center, New York, NY, USA. [10]Department of Immunology, Sloan Kettering Institute, New York, NY, USA. [11]Institute for Medical Microbiology, Immunology and Hygiene, School of Medicine, Technical University of Munich, Munich, Germany. [12]Comparative Experimental Pathology, School of Medicine, Technical University of Munich, Munich, Germany. [13]Institute of Pathology, School of Medicine, Technical University of Munich, Munich, Germany. [14]Department of Internal Medicine II, University Hospital, Ludwig-Maximilians-Universität, Munich, Germany. [15]German Center for Infection Research (DZIF), partner site Munich, Munich, Germany. [16]Bavarian Center for Biomolecular Mass Spectrometry, School of Life Sciences, Technical University of Munich, Freising, Germany. [17]Department of Radiation Oncology, School of Medicine, Technical University of Munich (TUM), Klinikum rechts der Isar TUM, Munich, Germany. [18]Department of Surgery, School of Medicine, Technical University of Munich (TUM), Klinikum rechts der Isar TUM, Munich, Germany. [19]Department of Internal Medicine II, University Medical Center, Freiburg, Germany. [20]Institute of Clinical Chemistry and Pathobiochemistry, School of Medicine, Technical University of Munich, Munich, Germany. [21]Department of Medicine, Memorial Sloan Kettering Cancer Center, New York, NY, USA. [22]Weill Cornell Medical College, New York, NY, USA. [23]Bavarian Cancer Research Center (BZKF), Munich, Germany. [24]Bavarian Cancer Research Center (BZKF), Regensburg, Germany. [25]These authors contributed equally: Erik Thiele Orberg, Elisabeth Meedt, Andreas Hiergeist, Jinling Xue, André Gessner, Li Deng, Ernst Holler, Hendrik Poeck. ✉e-mail: e.orberg@tum.de; hendrik.poeck@ukr.de

https://doi.org/10.1038/s43018-023-00669-x

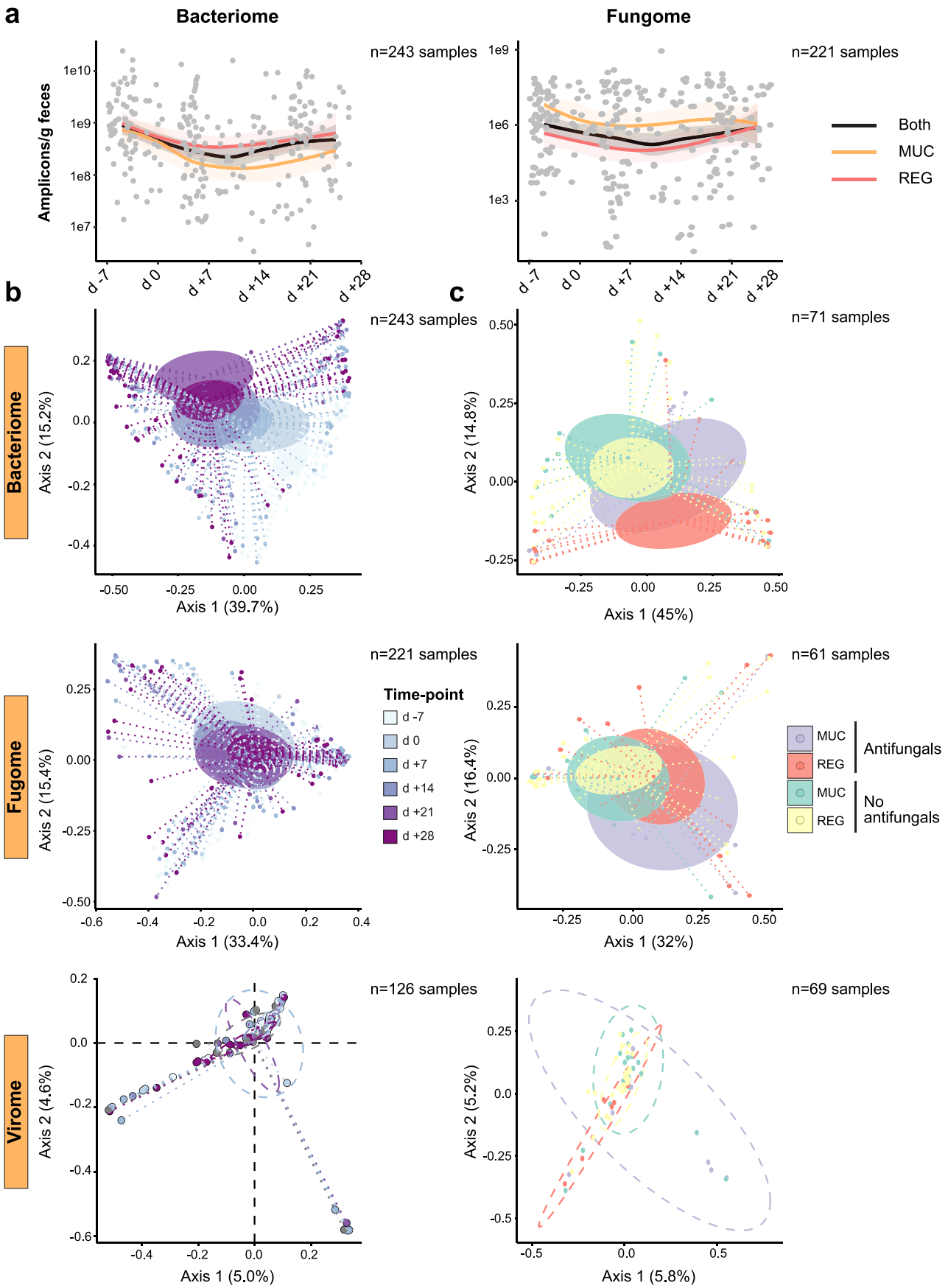

Extended Data Fig. 1 | See next page for caption.

https://doi.org/10.1038/s43018-023-00669-x

Extended Data Fig. 1 | Longitudinal dynamics of bacterial, fungal and viral community compositions in patients receiving allo-SCT. a) Quantification of the bacterial and fungal load by 16S and 28S rDNA copy numbers per gram of stool at time-points relative to all-SCT (Day 0). Solid lines represent the smoothed conditional means for the entire cohort (black), Munich (MUC, orange) or Regensburg (REG, red) calculated by locally weighted regression using the locally estimated scatterplot smoothing (LOESS) method. The gray shading indicates the 95% confidence interval for entire cohort. Each individual patient stool sample is plotted as a gray dot superimposed on the graph. The number of samples is indicated. **b**) Beta diversity analysis illustrating changes in bacteriome, fungome and virome by time-points relative to allo-SCT (Day 0). For bacteriome and fungome, beta diversity was calculated by weighted UniFrac. For virome, beta diversity was calculated by Bray-Curtis dissimilarity. Distances were projected in Principal coordinate analysis (PCoA). Bacteriome: Comparisons between Day +7 ($p = 0.001$), Day + 14 ($p = 0.001$), Day +21 ($p = 0.001$), Day +28 ($p = 0.001$) vs baseline (Day −7) are significant (pairwise Adonis test adjusted for multiple comparisons). Virome: Comparisons between Day +7 ($p = 0.013$) and Day +28 ($p = 0.001$) vs baseline are significant (PERMANOVA test). The number of samples is indicated. **c**) Beta diversity analysis illustrating changes in bacteriome, fungome and virome according to study center (MUC or REG) and whether patients received antifungal therapy ('No Antifungals' or 'Antifungals'). For bacteriome and virome, beta diversity was calculated by weighted UniFrac. For virome, beta diversity was calculated by Bray-Curtis dissimilarity. Distances were projected in Principal coordinate analysis (PCoA). The number of samples is indicated.

https://doi.org/10.1038/s43018-023-00669-x

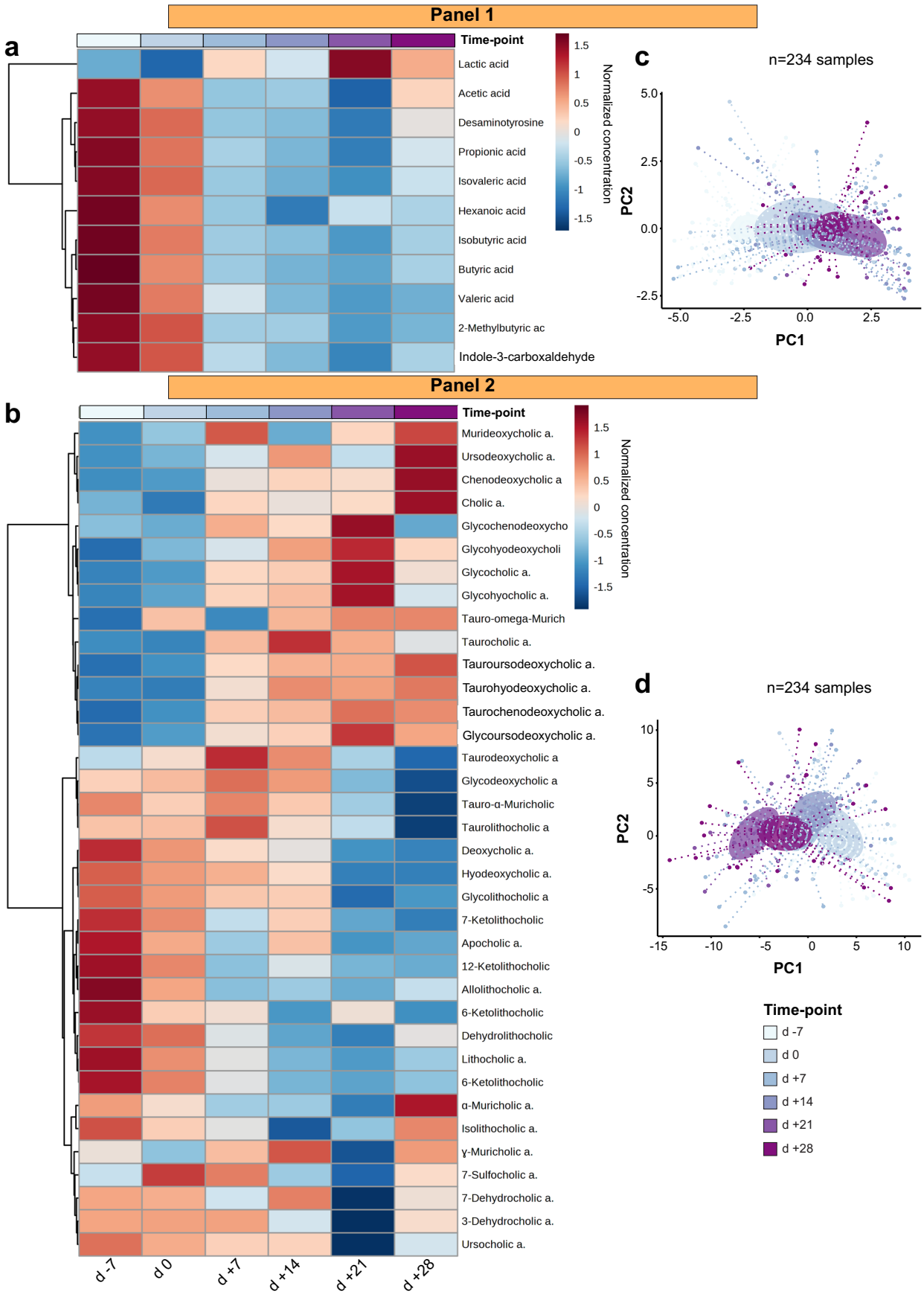

Extended Data Fig. 2 | See next page for caption.

https://doi.org/10.1038/s43018-023-00669-x

Extended Data Fig. 2 | Longitudinal dynamics of SCFAs, BCFAs, IIMs, PBAs and SBAs in patients receiving in allo-SCT. a) Heatmap of normalized Panel 1 metabolite levels in stool samples of allo-SCT patients averaged by time-points relative to allo-SCT. Normalized concentrations are indicated in the adjacent color legend. Clustering based on metabolite expression patterns using the Ward algorithm. Distance measure is Euclidian. The number of samples is indicated. **b)** Heatmap of normalized Panel 2 metabolite levels in stool samples of allo-SCT patients averaged by time-points relative to allo-SCT. Normalized concentrations are indicated in the adjacent color legend. Clustering based on metabolite expression patterns using the Ward algorithm. Distance measure is Euclidian. The number of samples is indicated. **c)** Principal component analysis (PCA) of Panel 1 metabolite profiles by time-points relative to allo-SCT. Comparisons at Day 0 ($p = 0.004$), Day +7 ($p = 0.001$), Day +14 ($p = 0.001$), Day +21 ($p = 0.001$) and Day +28 ($p = 0.001$) vs Day -7 are significant (pairwise Adonis test of Euclidean distances adjusted for multiple comparisons). **d)** PCA of Panel 2 metabolite profiles by time-points relative to allo-SCT. Comparisons at Day +7 ($p = 0.001$), Day +14 ($p = 0.001$), Day +21 ($p = 0.001$) and Day +28 ($p = 0.001$) vs Day −7 are significant (pairwise Adonis test of Euclidean distances adjusted for multiple comparisons).

https://doi.org/10.1038/s43018-023-00669-x

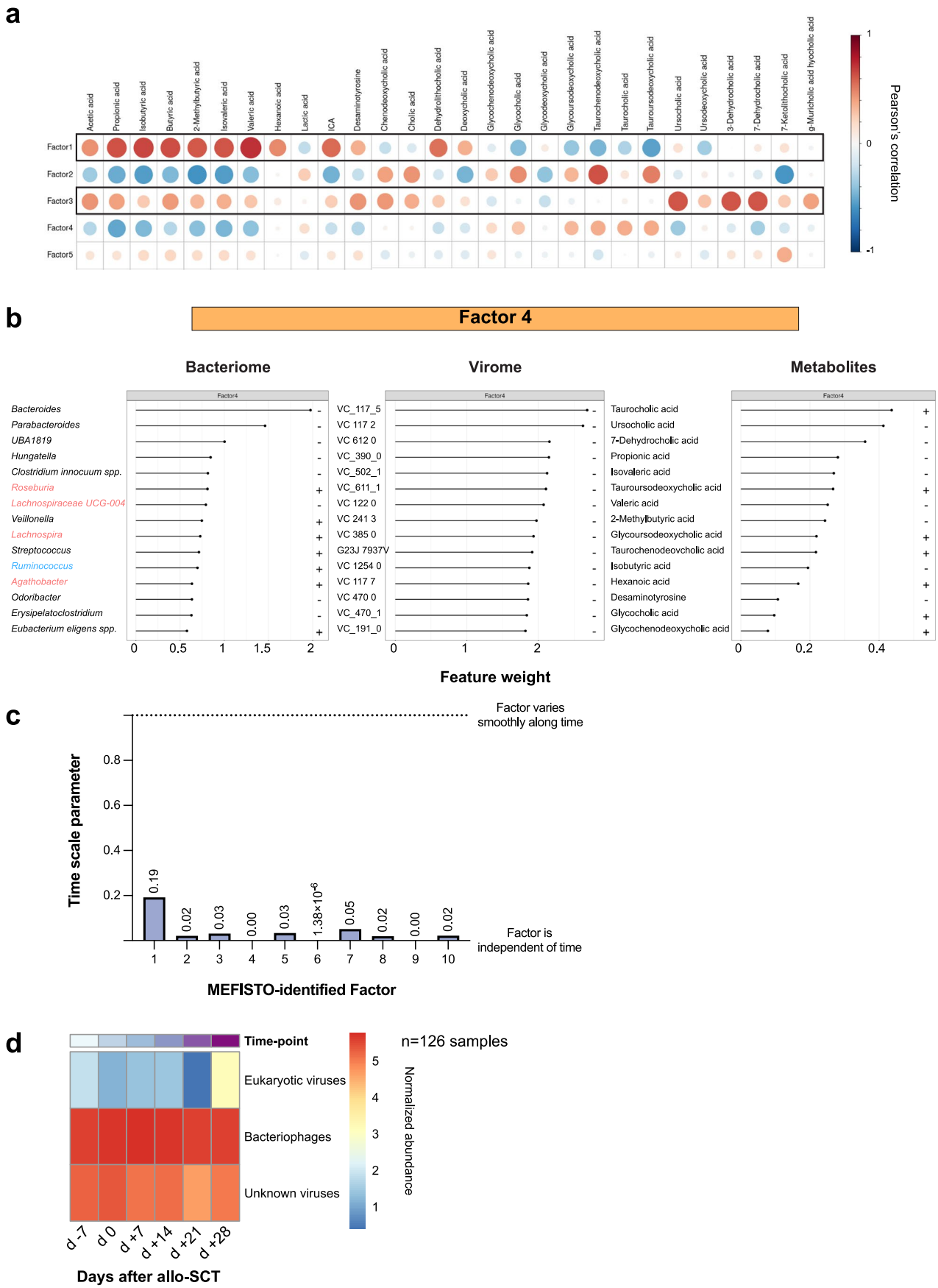

Extended Data Fig. 3 | See next page for caption.

https://doi.org/10.1038/s43018-023-00669-x

Extended Data Fig. 3 | MOFA (multi-omics factor analysis) and MEFISTO (a method for the functional integration of spatial omics data) in allo-SCT patients. a) Correlation between MOFA-identified Factors and normalized intestinal metabolite concentrations. Associations between Factor values and metabolites were analyzed via Pearson's correlation. The correlation coefficient is indicated in the adjacent color legend. The p-values associated with the correlations were corrected for multiple testing with the FDR approach. **b)** Top 15 Features in bacteriome, virome and metabolites in Factor 4 in descending order according to Feature weight. Larger weights indicate a higher correlation with that Factor, while the positive or negative sign indicates the directionality of that variation, that is, '+' indicates a positive association, '−' a negative association. **c)** Bar plot of time scale parameters assigned to Factors 1 through 10 identified by MEFISTO. MEFISTO assigns a time scale value between 0 and 1 to each Factor, which reflects the degree to which that Factor is dependent on time. A value of 0 implies no time-dependency, a value of 1 strong time-dependency. Of note, results pertaining to the identified Factors, their weight/covariance structure, variance explained across omics entities and Factor values obtained by MEFISTO modelling were almost identical and thus comparable to the output of our original MOFA model. **d)** Heatmap of normalized abundance of viral contigs assigned to eukaryotic and prokaryotic viruses at time-points relative to allo-SCT. The number of samples is indicated.

https://doi.org/10.1038/s43018-023-00669-x

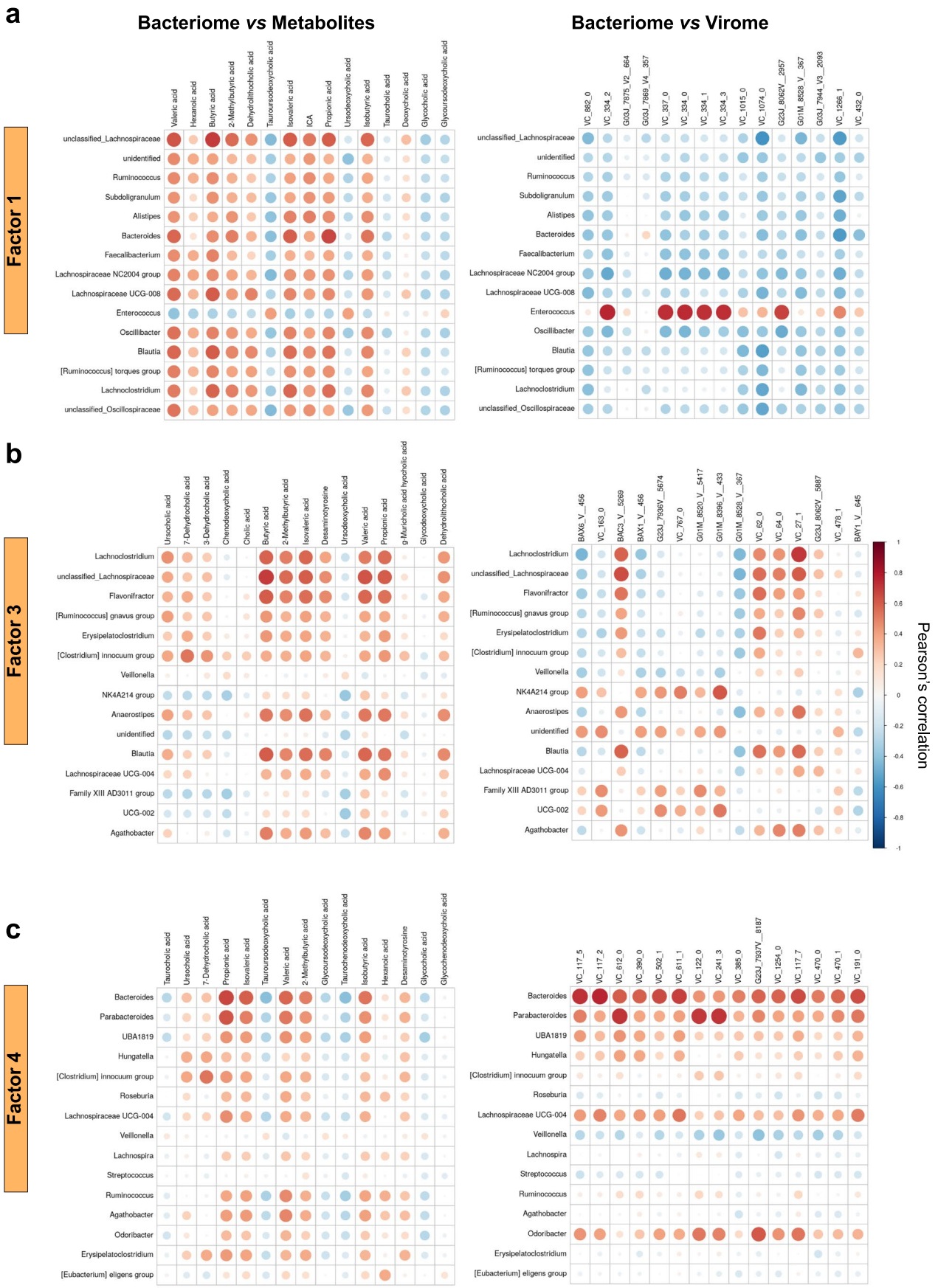

Extended Data Fig. 4 | See next page for caption.

https://doi.org/10.1038/s43018-023-00669-x

Extended Data Fig. 4 | Correlation between top 15 bacterial and metabolite as well as bacterial and viral high-weight Features in Factors 1, 3 and 4. **a)** Heatmaps of pairwise Pearson's correlations of top Features across different omics modalities. The Feature values of the top 15 high-weight Features of a given omics modality were correlated with that of another omics modality. (Left) bacterial taxa at genus level and metabolites, (right) bacterial taxa at genus level and bacteriophages at species level. The correlation coefficient is indicated in the adjacent color legend. The p-values associated with Pearson correlation have been corrected for multiple testing by applying the FDR approach to each set of correlations of two omics modalities of a given Factor. **b)** As in a) for Factor 3. **c)** As in a) for Factor 4.

https://doi.org/10.1038/s43018-023-00669-x

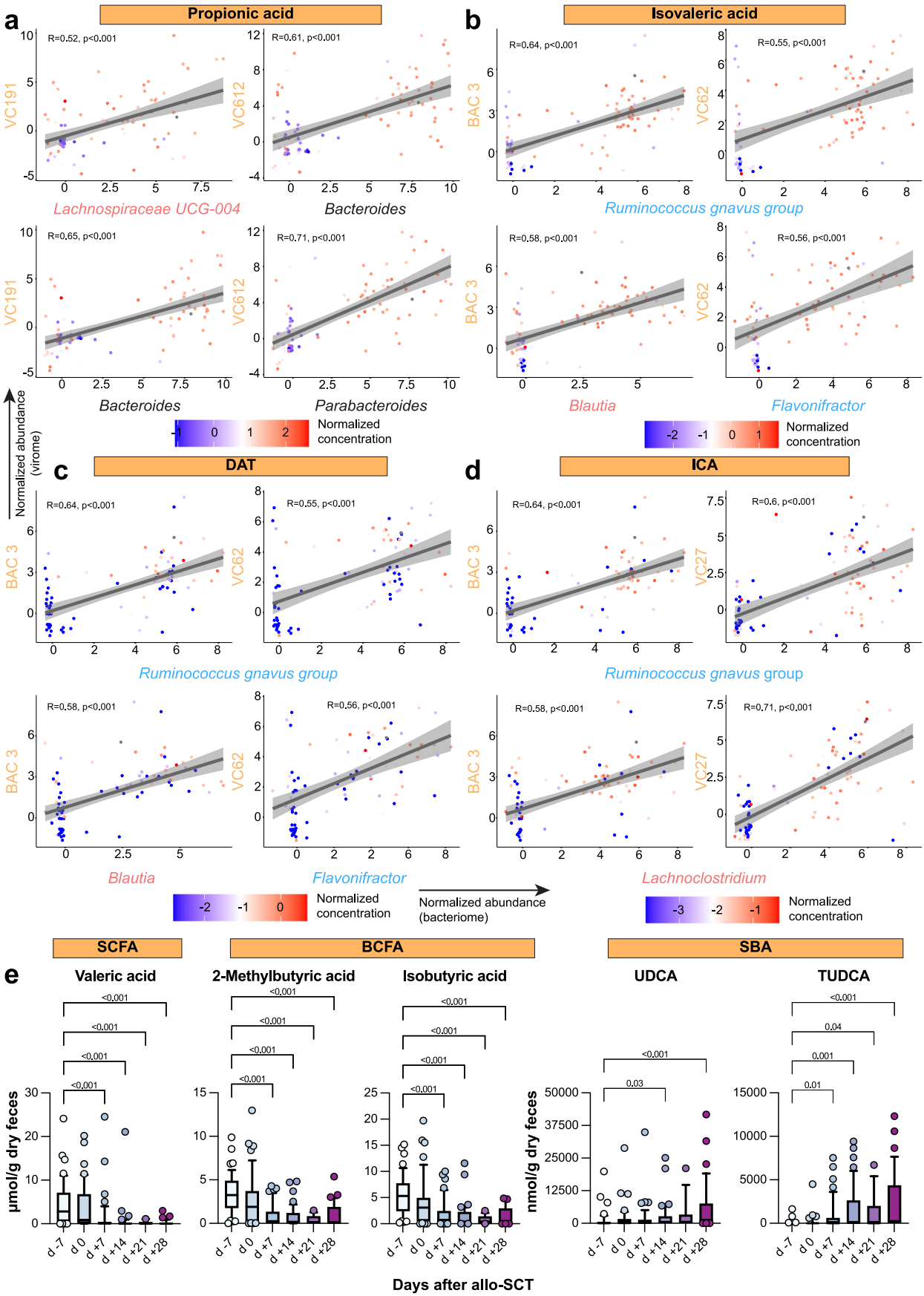

Extended Data Fig. 5 | See next page for caption.

https://doi.org/10.1038/s43018-023-00669-x

Extended Data Fig. 5 | Co-abundance of MOFA-identified bacterial and viral Features is associated with high-level IMM expression, which declines progressively after allo-SCT. a) Correlation scatter plots of high-weight Features within Factor 4, comparing normalized abundance of bacterial taxa at genus level (x-axis) with that of bacteriophages at species level (y-axis) together with the metabolite propionic acid. Dots represent samples from individual patients at different time points (91 samples from 45 patients), all of which had both 16S and viral metagenomic sequencing data. Dots are colored by intestinal levels of propionic acid, or in grey if no propionic acid data was available. Normalized concentrations of metabolites are indicated in the adjacent heatmap. Associations between bacterial genera and viral species were analyzed via Pearson correlation and linear regression. The R- and p-values are indicated in each plot. The regression line is drawn in blue and the 95 % confidence interval of the regression line is shaded in grey. **b)** As in a) for Features in Factor 3 and the metabolite isovaleric acid. **c)** As in a) for Features in Factor 3 and the metabolite DAT. **d)** As in a) for Features in Factor 3 and the metabolite ICA. **e)** Levels of intestinal microbiota-derived metabolites at time-points relative to allo-SCT (Day 0) in µmol per gram of dried stool measured by targeted mass spectrometry. Number of patients per time-point is indicated in Fig. 4d. Significance by two-sided Kruskal-Wallis test corrected for multiple testing via Dunn's test of all time-points against baseline (Day -7). In the box plots, the box ranges from the 25th to 75th percentiles. The line in the middle of the box is plotted at the median. The whiskers are drawn down to the 10th and up to the 90th percentile. Points below and above the whiskers are drawn as individual points. Points indicate individual patient stool samples sampled at the specified time-points. SBA…secondary bile acids; UDCA…ursodeoxycholic acid; TUDCA…tauroursodeoxycholic acid.

https://doi.org/10.1038/s43018-023-00669-x

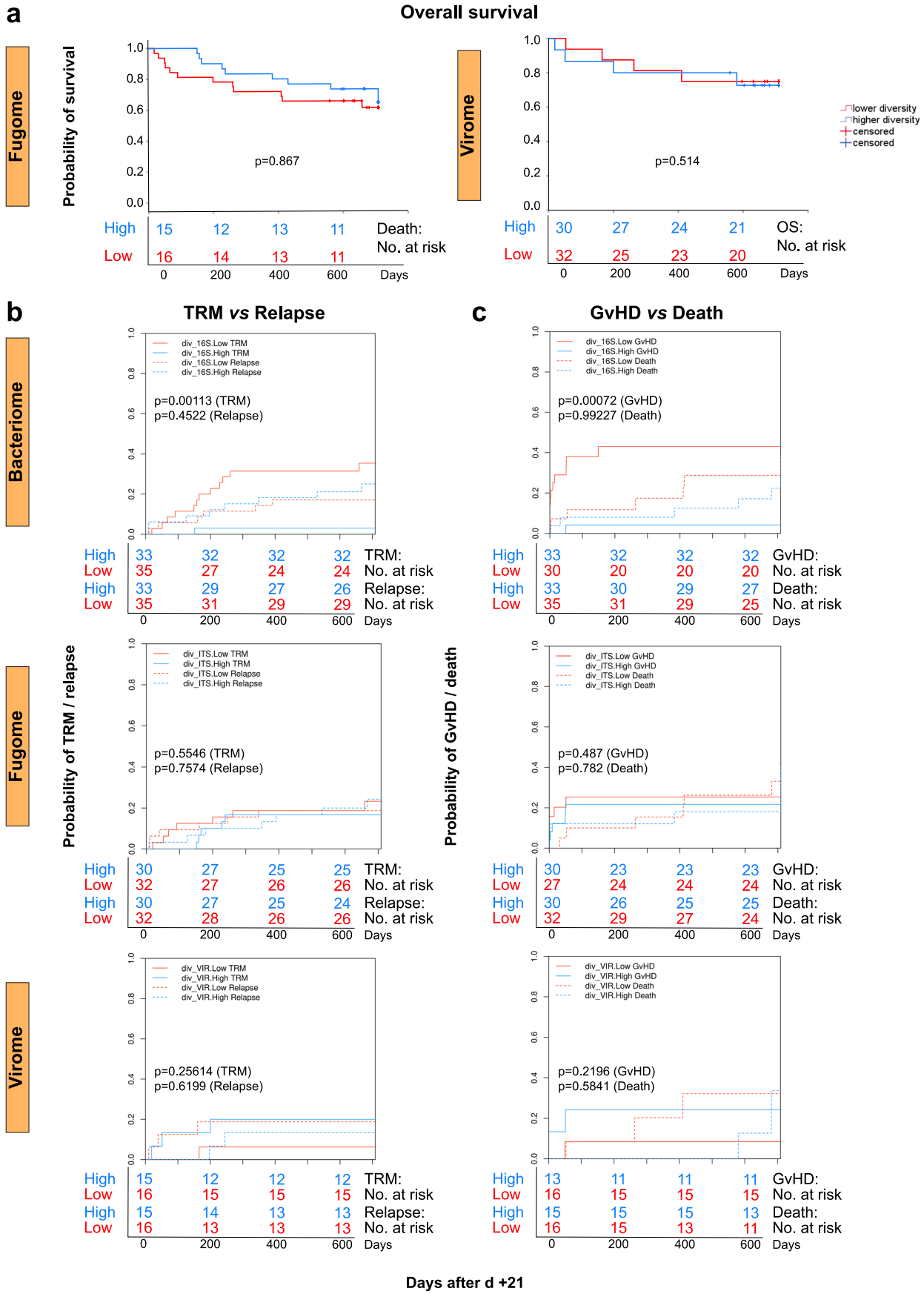

Extended Data Fig. 6 | See next page for caption.

https://doi.org/10.1038/s43018-023-00669-x

Extended Data Fig. 6 | Intestinal bacterial but not fungal nor viral diversity predicts outcome after allo-SCT. a) 2-year OS after Day 21 stratified according to higher and lower fungal (left) and viral (right) alpha diversity. The mean alpha diversity of patient samples at Days +7–21 was calculated and patients were stratified into higher (blue curve) and lower (red curve) diversity groups, defined as above or below the center-specific median Inverse Simpson's diversity index. For fungome, there were 12 deaths among 32 patients in the lower-diversity group (estimated mean survival time 521 (95% CI 428-614) days) and 10 deaths among 30 patients in the higher-diversity group (estimated mean survival time 597 (95% CI 522-672) days). For virome, there were 4 deaths among 16 patients in the lower-diversity group (estimated mean survival time 587 (95% CI 479-696) days) and 4 deaths among 15 patients in the higher-diversity group (estimated mean survival time 576 (95% CI 450-701) days). Analysis via Kaplan–Meier estimator, significance according to the log-rank test. **b)** 2-year cumulative incidence of relapse and transplantation-related mortality (TRM) in a competing risks analysis stratified according to higher and lower bacterial (top), fungal (middle) and viral (bottom) alpha diversity, calculated as in a). For bacteriome, there were 12 cases of TRM and 6 relapses among 35 patients in the lower-diversity group and one case of TRM and 8 relapses among 33 patients in the higher-diversity group. For fungome, there were 7 cases of TRM and 6 relapses among 32 patients in the lower-diversity group and 5 cases of TRM and 7 relapses among 30 patients in the lower-diversity. For virome, there was one case of TRM and 3 relapses among 16 patients in the lower-diversity group and 3 cases of TRM and 2 relapses among 15 patients in the higher-diversity. Significance according to Gray's test. **c)** 2-year cumulative incidence of GvHD and its competing risk Death in a competing risks analysis stratified by alpha diversity as in a). For bacteriome, there were 12 cases of GvHD and 6 deaths among 35 patients in the lower-diversity group and 1 case of GvHD and 8 deaths among 33 patients in the higher-diversity group. For fungome, there were 7 cases of GvHD and 6 deaths among 32 patients in the lower-diversity group and 5 cases of GvHD and 7 deaths among 30 patients in the lower-diversity group. For virome, there was one case of GvHD and 3 deaths among 16 patients in the lower-diversity group and 3 cases of GvHD and 2 deaths among 15 patients in the higher-diversity group. Statistics as in b).

https://doi.org/10.1038/s43018-023-00669-x

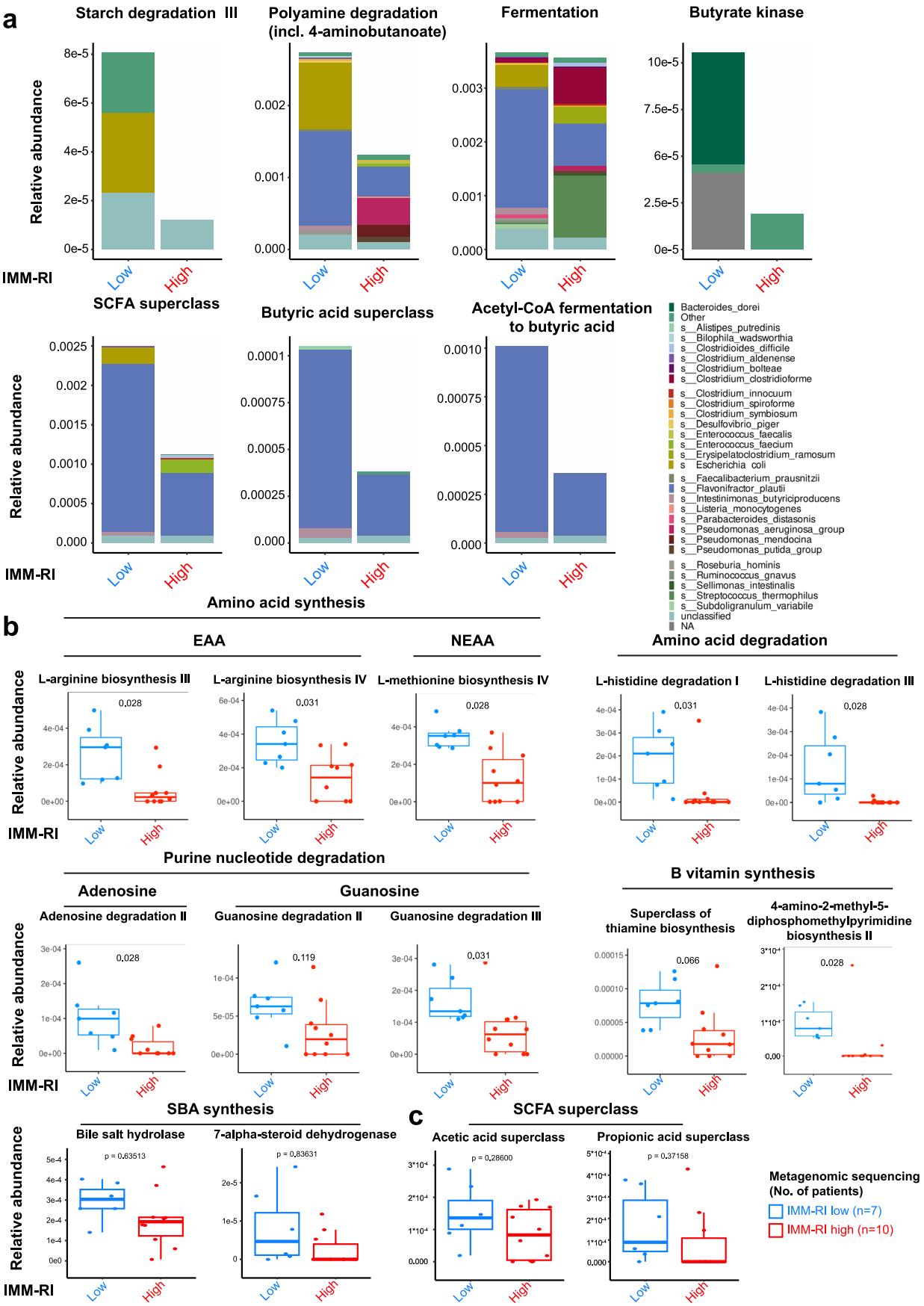

Extended Data Fig. 7 | See next page for caption.

https://doi.org/10.1038/s43018-023-00669-x

Extended Data Fig. 7 | Characterization of differentially abundant microbial pathways and the species which encode them in IMM-RI low- vs high-risk patients via whole shotgun metagenomic sequencing. a) Species-level association with MetaCyc pathways differentially abundant between IMM-RI low and high-risk patients (as shown in Fig. 6). The relative abundance and species-level identity of taxa encoding the indicated MetaCyc pathways are shown. **b)** Box plot of relative abundance of indicated MetaCyc pathways in IMM-RI low- vs high-risk patients. In the box plots, the box ranges from the 25th to 75th percentiles. The line in the middle of the box is plotted at the mean. The whiskers are drawn down to the minimum and up to the maximum. Samples outside the 1.5-fold IQR were regarded as outliers. Patient samples are plotted as a point superimposed on the graph (high IMM-RI: n = 10 patients; low IMM-RI: n = 7 patients). Significance by 1-sided Wilcoxon Rank Sum Test corrected for multiple comparisons via the Benjamini & Hochberg correction for multiple testing. **c)** Box plot of relative abundance of acetic acid and propionic acid superclasses in IMM-RI low- vs high-risk patients. Plots, numbers and statistics as in b).

https://doi.org/10.1038/s43018-023-00669-x

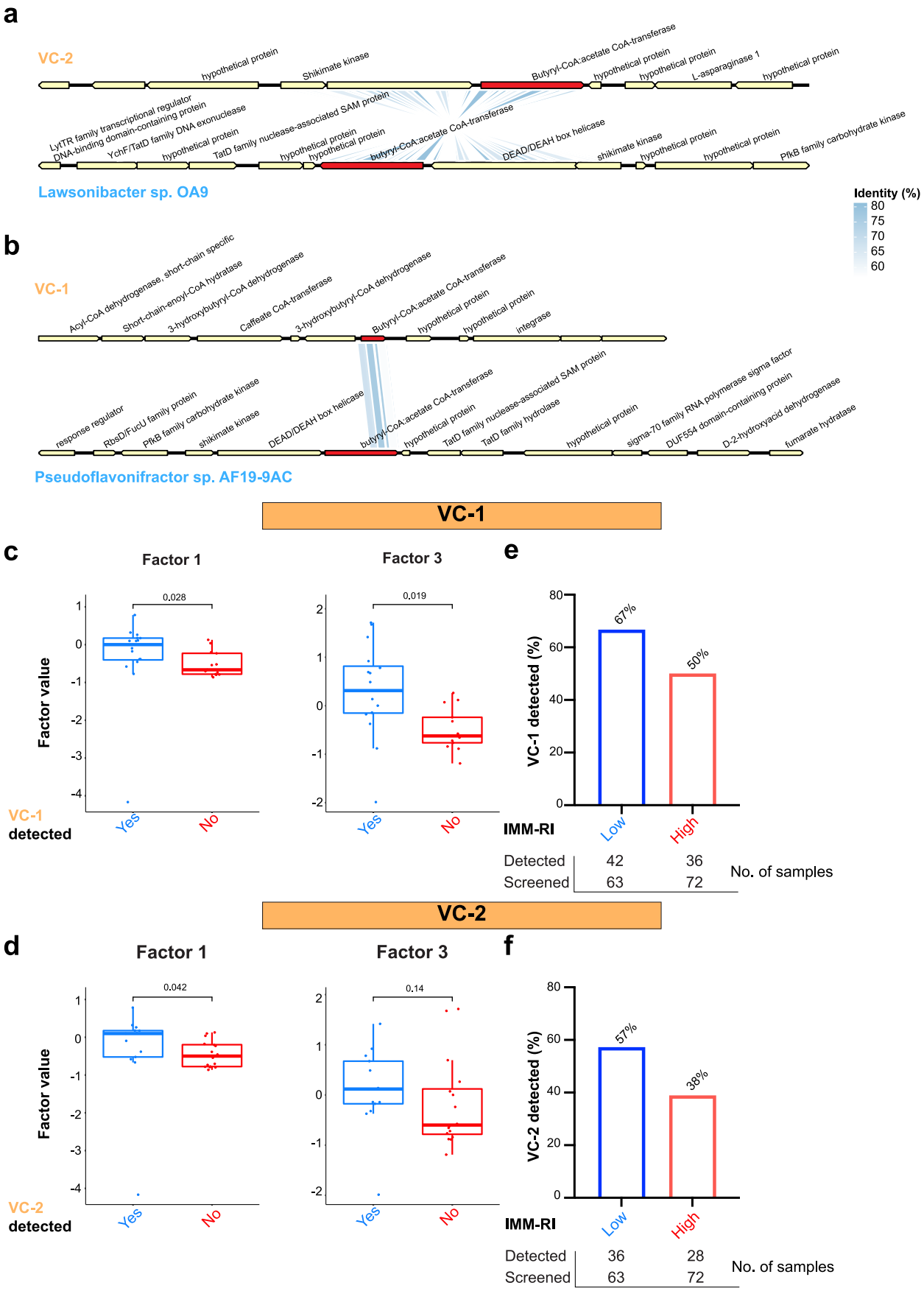

Extended Data Fig. 8 | See next page for caption.

https://doi.org/10.1038/s43018-023-00669-x

Extended Data Fig. 8 | *BCoAT*-coding VC-1 and VC-2 bacteriophages are associated with MOFA Factors 1 and 3 and the IMM-RI. a) Gene alignment plot of VC-2. The identity overlap (in percent) is indicated in the adjacent color legend. The *BCoAT* AMG is highlighted in red. **b)** Gene alignment plot of VC-1 as in a). **c)** Box plots of Factor values for Factors 1 and 3 (averaged across time-points Days +7–21) according to whether VC-1 was detected by viral metagenomic sequencing ('Yes') or not ('No'). The center line corresponds to the median, the box ranges from the 25th to the 75th percentile. Whisker length corresponds to the largest/lowest data point that does not exceed the 75th/25th percentile +/− 1.5-fold IQR. Blue: detected (n = 16 patients); red: not detected (n = 13 patients). Significance by two-tailed Mann-Whitney-U-test corrected for multiple testing via FDR. **d)** As in c) for VC-2. Blue: detected (n = 13 patients); red: not detected (n = 16 patients). **e)** Detection of the *BCoAT*-coding VC-1 in patient samples stratified according to IMM-RI. Bar plots show percentage, exact values are provided. The numbers of samples screened vs those in which *VC-1* was detected is indicated below. **f)** As in e) for VC-2.

https://doi.org/10.1038/s43018-023-00669-x

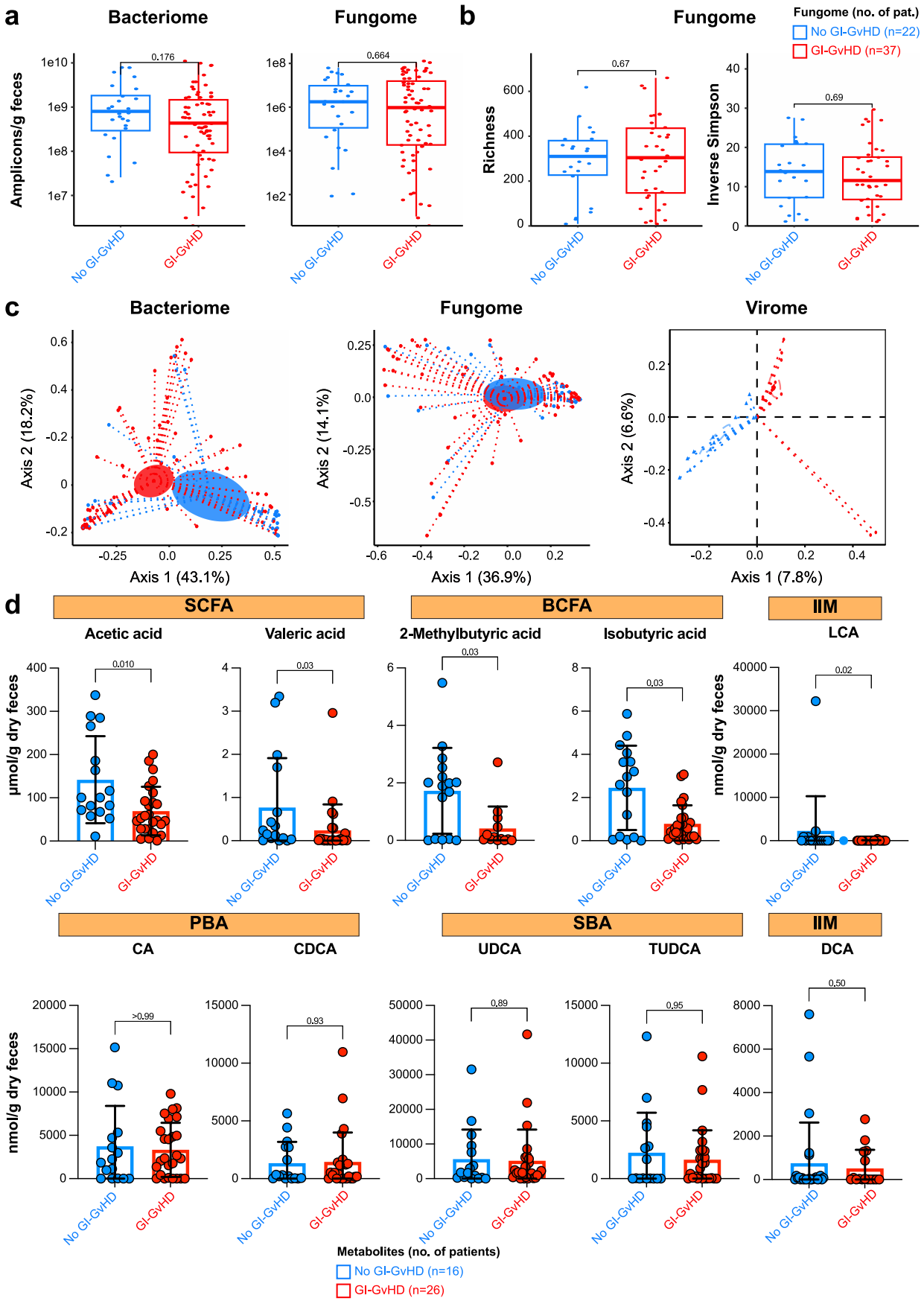

Extended Data Fig. 9 | See next page for caption.

https://doi.org/10.1038/s43018-023-00669-x

Extended Data Fig. 9 | Onset of acute GI-GvHD shifts intestinal bacterial and viral communities and impacts IMM expression profiles. a) Quantification of the bacterial and fungal load by 16S and 28S rDNA copy numbers per gram of stool stratified by patients diagnosed with GI-GvHD (GI-GvHD, red) vs control allo-SCT patients (No GI-GvHD, blue). The box ranges from the 25th to 75th percentiles. The line in the middle of the box is plotted at the median. The whiskers are drawn down to the minimum and maximum. Samples outside the 1.5-fold IQR were regarded as outliers. Significance by two-tailed Wilcoxon rank sum test adjusted for multiple comparisons via the Benjamini & Hochberg procedure. Each individual patient is plotted as a point superimposed on the graph. Number of patients: for 16S & 28S n = 22 vs n = 37, corresponding to 'No GI-GvHD' vs 'GvHD', respectively. **b)** Intestinal fungal alpha diversity (Richness, Inverse Simpson's diversity index) stratified by patients diagnosed with GI-GvHD (GI-GvHD) vs control allo-SCT patients (No GI-GvHD). Plots, numbers and statistics as in a). **c)** Beta diversity analysis illustrating changes in bacteriome, fungome and virome in patients with GI-GvHD vs control allo-SCT patients. For bacteriome and fungome, beta diversity was calculated by weighted UniFrac. For virome, beta diversity was calculated by Bray-Curtis dissimilarity. Distances were projected in PCoA. Bacteriome: Comparison between patients with GI-GvHD vs No GI-GvHD is significant ($p = 0.026$ by one-side pairwise Adonis test). Virome: Comparison between patients with GI-GvHD vs No GI-GvHD is significant ($p = 0.03$ by PERMANOVA test). **d)** Levels of indicated microbiota-derived metabolites stratified by patients diagnosed with GI-GvHD vs control allo-SCT patients. Significance by two-tailed Mann-Whitney test. In the scatter-dot plots, the box is plotted at the mean. Error bars indicate standard deviation. Each individual patient is plotted as a point superimposed on the graph. The number of patients per group are indicated in the legend.

https://doi.org/10.1038/s43018-023-00669-x

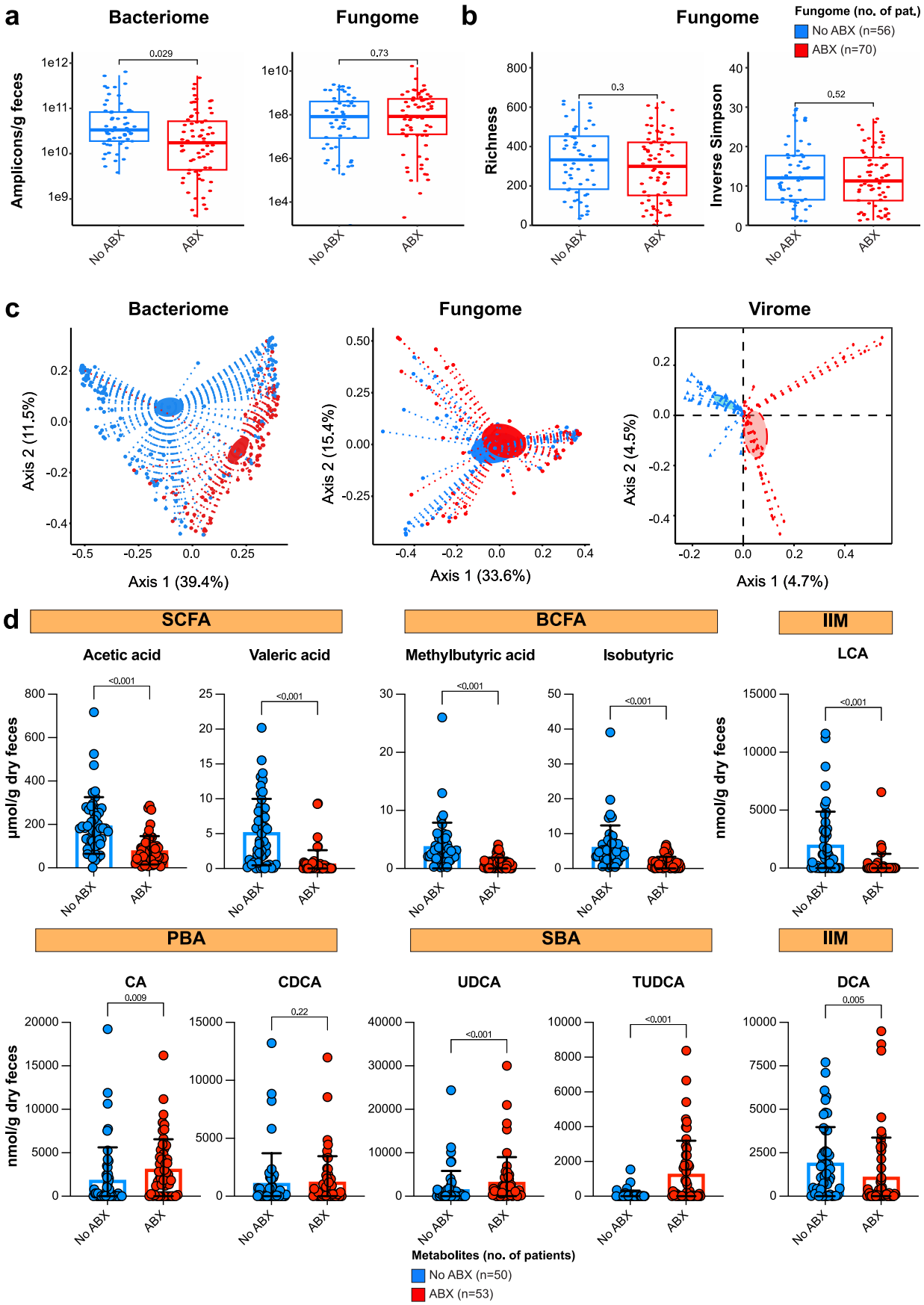

Extended Data Fig. 10 | See next page for caption.

https://doi.org/10.1038/s43018-023-00669-x

Extended Data Fig. 10 | Impact of antibiotics on bacterial abundance, bacterial and viral community composition and IMM expression profiles. **a)** Quantification of the bacterial and fungal load by 16S and 28S rDNA copy numbers per gram of stool stratified by antibiotic exposure: No Antibiotics ('No ABX', blue) (blue) vs Antibiotics ('ABX', red). Once a patient was treated with antibiotics, the current and all subsequent samples were classified as 'ABX'. The box ranges from the 25th to 75th percentiles. The line in the middle of the box is plotted at the median. The whiskers are drawn down to the minimum and maximum. Samples outside the 1.5-fold IQR were regarded as outliers. Significance by two-tailed Wilcoxon rank sum test adjusted for multiple comparisons via the Benjamini & Hochberg procedure. Each individual patient is plotted as a point superimposed on the graph. Number of patients: for 16S n = 59 vs n = 70, for 28S n = 56 vs n = 70, corresponding to 'No ABX' vs 'ABX', respectively. **b)** Intestinal fungal alpha diversity (Richness, Inverse Simpson's diversity index) in paired patient samples according to antibiotic status as in a). Plots, numbers and statistics as in a). **c)** Beta diversity analysis illustrating the impact of antibiotics on the intestinal bacterial, fungal and viral communities. Each point represents individual patient samples annotated with metadata regarding concomitant antibiotic therapy. For bacteriome and virome, beta diversity was calculated by weighted UniFrac. For virome, beta diversity was calculated by Bray-Curtis dissimilarity. Distances were projected in PCoA. Bacteriome: Comparison between patients with 'No ABX' vs 'ABX' is significant ($p = 0.001$ by one-side pairwise Adonis test). Virome: Comparison between patients with 'No ABX' vs 'ABX' is significant ($p = 0.003$ by PERMANOVA test). **d)** Levels of indicated microbiota-derived metabolites in paired patient samples before and after exposure to ABX. Significance by two-tailed Wilcoxon matched-pairs signed rank test. In the scatter-dot plots, the box is plotted at the mean. Error bars indicate standard deviation. Each individual patient is plotted as a point superimposed on the graph. The number of patients per group are indicated in the legend.

nature portfolio

Corresponding author(s): Erik Thiele Orberg, MD, PhD
Hendrik Poeck, MD

Last updated by author(s): 08/24/2023

Reporting Summary

Nature Portfolio wishes to improve the reproducibility of the work that we publish. This form provides structure for consistency and transparency in reporting. For further information on Nature Portfolio policies, see our Editorial Policies and the Editorial Policy Checklist.

Statistics

For all statistical analyses, confirm that the following items are present in the figure legend, table legend, main text, or Methods section.

n/a	Confirmed
☐	☒ The exact sample size (*n*) for each experimental group/condition, given as a discrete number and unit of measurement
☐	☒ A statement on whether measurements were taken from distinct samples or whether the same sample was measured repeatedly
☐	☒ The statistical test(s) used AND whether they are one- or two-sided *Only common tests should be described solely by name; describe more complex techniques in the Methods section.*
☐	☒ A description of all covariates tested
☐	☒ A description of any assumptions or corrections, such as tests of normality and adjustment for multiple comparisons
☐	☒ A full description of the statistical parameters including central tendency (e.g. means) or other basic estimates (e.g. regression coefficient) AND variation (e.g. standard deviation) or associated estimates of uncertainty (e.g. confidence intervals)
☐	☒ For null hypothesis testing, the test statistic (e.g. *F*, *t*, *r*) with confidence intervals, effect sizes, degrees of freedom and *P* value noted *Give P values as exact values whenever suitable.*
☒	☐ For Bayesian analysis, information on the choice of priors and Markov chain Monte Carlo settings
☐	☒ For hierarchical and complex designs, identification of the appropriate level for tests and full reporting of outcomes
☐	☒ Estimates of effect sizes (e.g. Cohen's *d*, Pearson's *r*), indicating how they were calculated

Our web collection on statistics for biologists contains articles on many of the points above.

Software and code

Policy information about availability of computer code

Data collection	Microbial sequencing data, metabolite expression profiles were collected from analysis platforms using Microsoft -Office-365 Excel (16.7.5) Clinical metadata was collected from patient electronic health records using Microsoft -Office-365 Excel (16.7.5)
Data analysis	Analyst 1.7 software (Sciex), bbmap suite (v38.76), bowtie2 (2.5.0), CAT (v5.0.4), CheckV, corrplot (0.91), CoverM (v0.6.1), cutadapt (3.4), dada2 (1.22), DECIPHER (2.26), dedupe.sh, DeepVirFinder (v1.0), fastp (v0.20.1), FastTree (2.1.1), ggplot2 (3.4.0), ggpubr (0.4.0), GraphPad Prism (9), HUMAnN (3.6), IBM SPSS 25, Maaslin2 (1.7.3), MAFFT (v7.475), Metaboanalyst (5.0), MetaPhlAn (4.0.3), meta SPAdes (v3.14.0), microbiomeMarker package (v1.0.1.), Microsoft Excel (16.7.5), minimap2, MMseqs2, MOFA2 (1.4.0), mofapy2 (0.6.4), MultiQuant 3.0.3 (Sciex, Darmstadt, Germany), pairwiseAdonis (v0.4), PHAMB, PHROGs, phyloseq (1.36), Prodigal (v2.6.3), Psych R (v2.1.9), pyCircus, Python (3.6.13), R (4.1.1), R (gggenomes package), R (ggtree package), R (vegan package), rstatix (0.7.0), tBLASTx, trimAl (v1.4.rev15), Trimmomatic (0.39), vConTACT2, ViroProfiler (v0.1), VirSorter2, vsearch (2.22.1)

For manuscripts utilizing custom algorithms or software that are central to the research but not yet described in published literature, software must be made available to editors and reviewers. We strongly encourage code deposition in a community repository (e.g. GitHub). See the Nature Portfolio guidelines for submitting code & software for further information.

Data

Policy information about availability of data

All manuscripts must include a data availability statement. This statement should provide the following information, where applicable:

- Accession codes, unique identifiers, or web links for publicly available datasets
- A description of any restrictions on data availability
- For clinical datasets or third party data, please ensure that the statement adheres to our policy

Microbial sequencing (bacterial, and fungal amplicon data and viral metagenomic sequencing data) that support the findings of this study have been deposited at the European Nucleotide Archive under accession number PRJEB53547 (https://www.ebi.ac.uk/ena/browser/view/PRJEB53547). Mass spectrometry data have been deposited at Zenodo under accession number 6603017 (https://zenodo.org/record/6603017). Both repositories are annotated with pseudonymized clinical metadata.
Code, scripts and packages used in the present study can be found at Github (https://github.com/guardianre/MOFA-in-allo-SCT.git).

Research involving human participants, their data, or biological material

Policy information about studies with human participants or human data. See also policy information about sex, gender (identity/presentation), and sexual orientation and race, ethnicity and racism.

Reporting on sex and gender	Findings reported in our study apply to both sexes. The study cohort included female and male patients and sex was assigned based on electronic patient records. Detailed numbers of patients in each sex is reported in Supplementary Table 1, male and female patients were equally distributed across both centers. We did not consider a priori sex- or gender-based analysis as they did not affect microbiome-predicted outcomes in published cohorts of allogeneic stem-cell transplantation patients (Taur et al., Blood 2014; Peled et al., NEJM 2020). We included sex as a covariate when comparing IMM-RI low- vs high-risk patients. However, we did not detect statistically significant differences between groups.
Reporting on race, ethnicity, or other socially relevant groupings	The study cohort included patients enrolled at the University Hospital Rechts der Isar in Munich and the University Hospital in Regensburg. Both centers are located in Bavaria, Germany and treat a populace that is largely of Western and Central European descent. In Munich, epidemiological data regarding place of birth of the patients and their parents was recorded, but race and ethnicity was not recorded a priori. In Regensburg, all patients identified as "Non-hispanic/white" based on self-reporting.
Population characteristics	Patient characteristics including age, sex, diagnosis, donor type, conditioning regimen, stem cell source, incidence of acute GI-GvHD, incidence of TRM, incidence of relapse, and 2-year overall survival are reported in Supplementary Table 1. If relapse or death occurred, the dates and cause of death were recorded. Patient characteristics according to IMM-RI are reported in the Supporting Information. Diet in Munich patients is reported in the Supporting Information. In patients with GI-GVHD, the onset, grade, treatment and outcome were recorded. In patients treated with anti-infective medication, antibiotics, antifungals or antivirals were recorded. We recorded type of antibiotics administered as per study-specific standards and the initiation of antibiotic treatment, this is reported in the Supporting Information.
Recruitment	At both centers, Munich and Regensburg, patients undergoing allogeneic stem-cell transplantation were enrolled (Munich: 2019-2021, Regensburg 2018-2021) in this prospective, observational cohort after obtaining informed consent and in accordance with IRB-approved study protocols (see "Ethics oversight"). All patients who were admitted for allo-SCT were screened for study enrollment. Stool samples were collected at predetermined time-points (calendar-driven, weekly from Day -7 until Day +35 or discharge, whichever occurred later) or in response to clinical occurrences (event-driven, e.g., onset of acute GI-GvHD). Patient were included in the analysis if a minimum of 3 longitudinal samples were available. We are not aware of a selection bias, since all patients were routinely screened for study participation, and the large majority of patients consented to study participation. There is a potential bias for inclusion of patients with a longer hospital stay in the analysis, since they are more likely to have met the minimum number of samples required.
Ethics oversight	Technical University of Munich, IRB 295/18 S; University of Regensburg, IRB 14-47_1-101, 14-101-0047, 21-2521-01.

Note that full information on the approval of the study protocol must also be provided in the manuscript.

Field-specific reporting

Please select the one below that is the best fit for your research. If you are not sure, read the appropriate sections before making your selection.

☒ Life sciences ☐ Behavioural & social sciences ☐ Ecological, evolutionary & environmental sciences

For a reference copy of the document with all sections, see nature.com/documents/nr-reporting-summary-flat.pdf

Life sciences study design

All studies must disclose on these points even when the disclosure is negative.

Sample size	Patients analyzed in this study were hospitalized for allo-SCT at the University Hospital rechts der Isar in Munich and the University Hospital Regensburg. Inclusion criteria were adult patients (18 years old or older) who received allo-SCT and had a collection of at least 3 longitudinal

	stool samples collected between hospital admission 1 weeks before and up to 5 weeks after allo-SCT. Our prospective objective was to include at least 70 patients based on the size of other published cohorts. Between 2018 and 2021, the 78 patients who fulfilled inclusion criteria were prospectively included in the study without any selection. A total of 356 stool samples were collected (see Figure 1). For this observational cohort, no a priori sample size calculation was performed. However, the size of our cohort (n=78) is similar to those reported in previous studies (Taur et al., Blood 2014).
Data exclusions	Exposure to broad-spectrum antibiotics was an a priori data exclusion criteria. Initiation of antibiotic therapy was recorded for all patient samples. Once a patient was started on antibiotics the first and all subsequent samples were excluded from the "No ABX" subset and classified as “ABX” for all subsequent analysis. Samples obtained after Day +100 after allo-SCT (n=2) were excluded from the analysis, since the microbiome at this late time-point is no longer comparable to that of the early post-transplant period.
Replication	We performed a cross-cohort analysis by comparing microbiome, microbiota-derived metabolites and clinical outcome within two German centers. The study population was well-balanced and there were no statistically significant differences in regard to age, gender, underlying disease, donor type, intensity of conditioning and incidence of GI-GvHD across both centers. We observed a difference between both centers in regard to survival (Munich 52%, Regensburg 72%), which are in the range of allo-SCT reported outcomes and may be explained in part by stem cell source. There were no differences in regard to TRM or relapse between centers. The association of bacterial microbiome diversity and clinical outcome confirmed those of published cohorts (Taur et al., Blood 2014; Peled et al., NEJM 2020).
Randomization	Patients were not randomized in different experimental groups, nor was there an active intervention. The clinical course (development of graft-versus-host disease, antibiotic therapy, high and low intestinal bacterial alpha diversity, high and low intestinal metabolite expression) determined the allocation to different subgroups.
Blinding	Investigators, technicians and analysts where blinded in regards to allocations to the different groups at the time of sample processing, next-generation amplicon and metagenomic sequencing and metabolomics mass-spectrometry.

Reporting for specific materials, systems and methods

We require information from authors about some types of materials, experimental systems and methods used in many studies. Here, indicate whether each material, system or method listed is relevant to your study. If you are not sure if a list item applies to your research, read the appropriate section before selecting a response.

Materials & experimental systems

n/a	Involved in the study
☒	☐ Antibodies
☒	☐ Eukaryotic cell lines
☒	☐ Palaeontology and archaeology
☒	☐ Animals and other organisms
☒	☐ Clinical data
☒	☐ Dual use research of concern
☒	☐ Plants

Methods

n/a	Involved in the study
☒	☐ ChIP-seq
☒	☐ Flow cytometry
☒	☐ MRI-based neuroimaging